XAP5 CIRCADIAN TIMEKEEPER regulates RNA splicing and the circadian clock via genetically separable pathways

Authors:

Hongtao Zhang (张弘韬)[1], Roderick W. Kumimoto[1], Shajahan Anver[1,2], Stacey L. Harmer[1*]

Author affiliations:

[1]Department of Plant Biology, College of Biological Sciences, University of California, Davis, CA 95616, USA

[2]Department of Genetics, Evolution and Environment, University College London, London, UK

[*]**Corresponding author:**

slharmer@ucdavis.edu

Running title:

Separable roles for *XCT* in splicing and the clock

One sentence summary:

XCT plays genetically separable roles in controlling the fidelity of 3' splice site selection during pre-mRNA splicing and the pace of circadian clock in Arabidopsis

Abstract

The circadian oscillator allows organisms to synchronize their cellular and physiological activities with diurnal environmental changes. In plants, the circadian clock is primarily composed of multiple transcriptional-translational feedback loops. Regulators of post-transcriptional events, such as pre-mRNA splicing factors, are also involved in controlling the pace of the clock. However, in most cases the underlying mechanisms remain unclear. We have previously identified *XAP5 CIRCADIAN TIMEKEEPER* (*XCT*) as an *Arabidopsis thaliana* circadian clock regulator with uncharacterized molecular functions. Here, we report that XCT physically interacts with components of the spliceosome, including members of the Nineteen Complex (NTC). PacBio Iso-Seq data show that *xct* mutants have transcriptome-wide pre-mRNA splicing defects, predominantly aberrant 3' splice site selection. Expression of a genomic copy of *XCT* fully rescues those splicing defects, demonstrating that functional *XCT* is important for splicing. Dawn-expressed genes are significantly enriched among those aberrantly spliced in *xct* mutants, suggesting that the splicing activity of *XCT* may be circadian regulated. Furthermore, we show that loss of function mutations in *PRP19A* or *PRP19B*, two homologous core NTC components, suppress the short circadian period phenotype of *xct-2*. However, we do not see rescue of the splicing defects of core clock genes in *prp19 xct* mutants. Therefore, our results suggest that *XCT* may regulate splicing and the clock function through genetically separable pathways.

Introduction

Most eukaryotes have evolved an endogenous timekeeper known as the circadian clock, which allows them to anticipate the daily fluctuating environmental conditions caused by the earth's rotation (Harmer, 2009). Although the central oscillators of circadian clocks in diverse eukaryotes lack conserved individual components, they share similar general architectures (Nohales and Kay, 2016). In plants, the approximately 24-h periodicity of the clock is maintained by a complex gene regulatory network consisting primarily of repressors and activators of transcription. Those regulators, often referred to as core circadian clock genes, regulate each other's expression and the expression of thousands of output genes (Creux and Harmer, 2019).

62 Additionally, post-transcriptional and post-translational mechanisms such as alternative splicing
63 of precursor messenger RNAs (pre-mRNAs) provide critical regulation of clock function. It has
64 been suggested that changes in splicing of core circadian clock genes are important for
65 Arabidopsis in response to environmental stresses (James et al., 2012; Kwon et al., 2014). For
66 example, cold temperatures significantly suppress production of a splice variant of *CIRCADIAN*
67 *CLOCK-ASSOCIATED1* (*CCA1*) in which intron four is retained. This incompletely spliced
68 isoform encodes a truncated protein which competitively inhibits the function of fully spliced
69 *CCA1* (Seo et al., 2012). However, in most cases the effects of alternative splicing of pre-
70 mRNAs on circadian clock function remain unclear.
71
72 In contrast, the mechanisms underlying pre-mRNA splicing are increasingly well understood
73 (Wilkinson et al., 2020). There are two catalytic transesterification steps, which sequentially
74 remove first the 5' and then the 3' splice sites (5'SS and 3'SS) of introns from their adjacent
75 exons (Shi, 2017). This process is carried out by five small nuclear ribonucleoproteins (snRNPs)
76 and hundreds of non-snRNP splicing factor proteins which assemble on a pre-mRNA to form the
77 spliceosome complex (Wilkinson et al., 2020). One of these spliceosome complex components is
78 the Nineteen Complex (NTC, also known as PRP19 complex), named after PRECURSOR RNA
79 PROCESSING 19 (PRP19), a U-box E3 ubiquitin ligase that forms the core of the NTC
80 (Hatakeyama et al., 2001; Koncz et al., 2012). The NTC is associated with the spliceosome
81 during the two transesterification steps and helps facilitate conformational rearrangements and
82 promote splicing fidelity (Fig. 1; Hogg et al., 2010). The NTC is highly conserved across
83 eukaryotes. In Arabidopsis, multiple orthologs of yeast NTC proteins including two PRP19
84 homologs (PRP19A/MAC3A and PRP19B/MAC3B) have been shown to physically interact
85 with the spliceosome (Monaghan et al., 2009; Deng et al., 2016). Plants mutant for *prp19a*
86 *prp19b* or homologs of other NTC-associated proteins such as *pleiotropic regulatory locus1*
87 (*prl1*) and *snw/ski-interacting protein* (*skip*) have genome-wide intron retention defects (Jia et al.,
88 2017; Wang et al., 2012; Li et al., 2019). These data indicate that NTC components act as
89 evolutionarily conserved splicing factors in Arabidopsis.
90
91 Mutation of splicing factors can lead to disruption of circadian clock function (Shakhmantsir and
92 Sehgal, 2019). For example, loss-of-function alleles of NTC components, including *PRP19*,

93 *PRL1* and *SKIP*, cause lengthening of circadian period (Wang et al., 2012; Feke et al., 2019; Li
94 et al., 2019). Aberrantly spliced mRNA variants of core circadian clock genes have been
95 detected in these splicing factor mutants (Sanchez et al., 2010; Wang et al., 2012; Jones et al.,
96 2012; Schlaen et al., 2015; Marshall et al., 2016; Li et al., 2019; Feke et al., 2019), suggesting
97 that changes in the pace of the clock might be caused by aberrant splicing of core clock genes. In
98 some cases, epistasis analysis suggests that this may be true (Marshall et al., 2016; Schlaen et al.,
99 2015). However, in other cases, genetic analysis has either not been performed or has revealed
100 additive interactions between the splicing factor and clock gene mutants. In addition, the levels
101 of mis-spliced mRNA variants of clock genes are usually only a small fraction of total transcripts
102 (Jones et al., 2012; Perez-Santángelo et al., 2014; Feke et al., 2019; Sanchez et al., 2010; Wang
103 et al., 2012). Thus, it is unclear whether splicing factors affect clock function solely by
104 controlling the splicing of core clock genes.
105
106 RNA splicing factors often function in multiple biological pathways: plants deficient for
107 components of the NTC have defects in immunity, microRNA biogenesis, DNA damage
108 response and transcriptional elongation (Koncz et al., 2012; Monaghan et al., 2009; Zhang et al.,
109 2013; Jia et al., 2017). Some splicing factors are known to carry out roles in nuclear processes
110 biochemically separable from their roles in splicing. In addition to its structural role in the
111 spliceosome, PRP19 also senses DNA damage and promotes DNA repair via its ubiquitin ligase
112 activity (Maréchal et al., 2014). Additionally, SKIP acts in two distinct complexes to regulate
113 splicing and the transcription of genes involved in flowering time control (Li et al., 2019).
114 Nonetheless, whether splicing factors might control circadian clock function via splicing-
115 independent activities has not been investigated.
116
117 We previously identified *XAP5 CIRCADIAN TIMEKEEPER* (*XCT*) as a novel regulator of the
118 Arabidopsis circadian clock (Martin-Tryon and Harmer, 2008). Like NTC components, XCT is
119 also well-conserved across eukaryotes. Homologs of XCT (also known as XAP5 proteins) share
120 a highly conserved C-terminal protein domain and are nuclear-localized (Martin-Tryon and
121 Harmer, 2008; Anver et al., 2014; Li et al., 2018; Lee et al., 2020). Previously, we found that
122 transgenic expression of Arabidopsis *XCT* fully rescued the slow-growth phenotype of fission

yeast mutant for *xap5* (Anver et al., 2014). Taken together, these data suggest that XCT homologs might share similar molecular and cellular functions across kingdoms.

It has been reported that FAM50A, one of the two XCT orthologs in humans, physically associates with the spliceosomal C complex and its mutants have defects in RNA splicing (Bessonov et al., 2008; Lee et al., 2020). Similarly, a recent study in Arabidopsis also reported the association of XCT with the spliceosome (Liu et al., 2022), implying that XAP5 proteins may be evolutionarily conserved splicing factors. However, evidence suggests that XAP5 proteins may also participate in fundamental biological processes other than splicing. Fission yeast and *Chlamydomonas* XAP5 proteins associate with chromatin and directly regulate transcription (Anver et al., 2014; Li et al., 2018). In addition to its role in the clock, Arabidopsis *XCT* has been implicated in diverse processes including small RNA production, immune signaling, and DNA damage responses (Fang et al., 2015; Xu et al., 2017; Kumimoto et al., 2021). Notably, NTC components have also been reported to function in all these pathways (Jia et al., 2017; Maréchal et al., 2014; Chanarat and Sträßer, 2013). Although pleiotropic defects are seen in *xct* mutants, interconnections between these phenotypes and the molecular function of *XCT* have not been extensively studied.

In the current work, we report that XCT physically interacts with NTC and other spliceosome-associated proteins in Arabidopsis. We use long-read RNA sequencing to reveal that *XCT* controls the fidelity of 3' splice site selection for hundreds of pre-mRNA splicing events, probably by rejecting downstream suboptimal 3' splice sites. Intriguingly, circadian-regulated genes that are aberrantly spliced in *xct* mutants are significantly enriched for peak expression at subjective dawn. This implies that the splicing-related activity of *XCT* may be circadian regulated. We also demonstrate that *PRP19A* and *PRP19B* display epistatic genetic interactions with *XCT* in control of the circadian clock period length but not of the splicing of core clock genes. This is consistent with our finding that although *xct-2* causes more severe splicing defects than *xct-1*, *xct-1* mutants have a stronger circadian phenotype. Collectively, our results suggest that XCT works close to NTC and may regulate pre-mRNA splicing and the circadian clock function via distinct pathways.

154 **Results**

155 **XCT physically interacts with the Nineteen Complex and other spliceosome-associated**
156 **proteins**

157

158 To uncover the molecular functions of XCT, we carried out mass spectrometry (MS)
159 experiments to identify its possible interactors. We expressed epitope-tagged XCT protein under
160 the control of the native *XCT* promoter in *xct-2* mutant background (*xct-2 XCT*). This transgene
161 largely rescued the morphological and circadian clock defects of *xct-2* (Supplemental Fig. 1).
162 Next, we affinity purified tagged XCT from plant extracts and analyzed co-purifying proteins via
163 MS. In total, 26 proteins were significantly enriched in the XCT immunoprecipitation compared
164 to control immunoprecipitations (Welch's two sample *t*-test, $P < 0.05$; Supplemental Dataset 1).
165 Among those XCT-associated proteins, 15 (57.7%) were annotated as mRNA splicing-related,
166 including 11 core NTC or NTC-associated proteins (Table 1), consistent with the MS and co-
167 immunoprecipitation data from a recent report (Liu et al., 2022). Notably, studies in human and
168 yeast have revealed that NTC is physically associated with the spliceosomal complex throughout
169 the two catalytic transesterification steps (Fig. 1; Hogg et al., 2010). Taken together, those results
170 imply that *XCT* may act close to NTC and function in the catalytic steps during pre-mRNA
171 splicing. Interestingly, we also observed 8 (30.8%) chloroplast proteins enriched in the XCT
172 immunoprecipitation (Supplemental Dataset 1), which may be related to the delayed leaf
173 greening phenotypes observed in *xct-2* mutant plants (Martin-Tryon and Harmer, 2008).

174

175 ***XCT* is required for the fidelity of 3' splice site selection during pre-mRNA splicing**

176

177 To investigate a possible role for *XCT* in RNA splicing, we performed PacBio Isoform
178 Sequencing (Iso-Seq) on wild-type Col-0, reduction-of-function allele *xct-1*, null allele *xct-2*, and
179 the complemented line *xct-2 XCT*. Additionally, we also sequenced *prl1-2*, which contains a T-
180 DNA insertion mutation *in PRL1*, an NTC member that has been demonstrated to control
181 genome-wide splicing efficiency (Jia et al., 2017). Since both transcript levels and RNA splicing
182 of a large proportion of the Arabidopsis transcriptome are circadian regulated (Romanowski et
183 al., 2020; Yang et al., 2020), the time of day at which plants are harvested has significant effects
184 on gene expression and splicing analysis (Hsu and Harmer, 2012). Therefore, we grew plants in

185 constant environmental conditions for ten days to desynchronize clocks of individual plants. To
186 further minimize any differences in subjective time of day between wild-type plants, the long-
187 circadian-period *prl1-2*, and the short-period *xct* mutants (Supplemental Fig. 2), we pooled
188 seedlings harvested at 2-hour intervals across a twenty-four hour period (Fig. 2A). For each
189 genotype, we sequenced three biological replicates and acquired an average of 784,832 full-
190 length transcript reads per genotype per replicate (Supplemental Dataset 2). With no alignment
191 needed, those reads were directly mapped to the TAIR 10 Arabidopsis reference genome and
192 then subjected to differential splicing analysis using the JunctionSeq R package (Hartley and
193 Mullikin, 2016).
194
195 Previous studies have demonstrated that intron retention is the most prevalent type of alternative
196 splicing event in Arabidopsis (Wang and Brendel, 2006; Filichkin et al., 2010). Indeed, plants
197 mutant for multiple NTC components have been reported to have global intron retention defects
198 (Jia et al., 2017; Meng et al., 2022). In our analysis of *prl1-2*, we found 5,730 out of 44,496
199 detected splicing events were significantly differentially enriched from Col-0 (Supplemental
200 Dataset 3). Notably, 99% of these events were decreases in known junctions (Supplemental Fig.
201 3), consistent with previous studies suggesting that loss of *PRL1* function mainly causes intron
202 retention without affecting splice site selection (Jia et al., 2017).
203
204 We next examined transcript composition in *xct* mutants. In the null allele *xct-2*, we detected
205 75,073 splicing events, of which 875 were significantly down-regulated and 532 were up-
206 regulated compared with Col-0 (FDR<0.05, Fig. 2B-C). Meanwhile, 209 and 337 splicing events
207 were significantly decreased or increased, respectively, in the partial loss-of-function mutant *xct-*
208 *1*. Comparing mis-regulated splicing between the two *xct* mutant alleles, 196 (93.8%) of the
209 down-regulated and 329 (97.6%) of the up-regulated events were shared. Thus, the two *xct*
210 alleles have similar splicing phenotypes but the severity of the defect is greater in the null allele
211 despite the stronger effect of *xct-1* on circadian period (Supplemental Fig. 1). Next, we analyzed
212 the splicing events in the complemented line *xct-2 XCT*. Only 16 out of 84,965 events were
213 significantly differentially enriched compared with Col-0, indicating that the splicing defects of
214 *xct-2* were almost completely rescued by the restored *XCT* expression. Taken together, these
215 results demonstrate that *XCT* is important for transcriptome-wide pre-mRNA splicing.

216

217 To further characterize the major types of splicing defects caused by loss of *XCT* function, we
218 analyzed the splice sites for the differentially spliced junctions in *xct* mutants. Specifically, we
219 categorized *xct*-induced mis-splicing events into four classes based on whether the 5' and 3'
220 splice sites used were previously annotated (known) or not (novel). As expected, most down-
221 regulated splicing events displayed decreases in usage of junctions with known 5' and 3' splice
222 sites (Fig. 2D). Interestingly, 307 (90.8%) in *xct-1* and 462 (86.5%) in *xct-2* of up-regulated
223 splicing events involved increased usage of junctions with a known 5' splice site but a novel 3'
224 splice site (Fig. 2E). The decreases in abundance of junctions with known splice sites hence
225 reflects both intron retention events and novel 3' splice sites usage. Therefore, our results
226 demonstrate that in addition to controlling the efficient removal of introns, *XCT* is also
227 responsible for the fidelity of 3' splice site selection.
228

229 To investigate how *XCT* contributes to the fidelity of 3' splice site selection, we compared the
230 significantly up- or down-regulated 3' splice sites in *xct* mutants with all detected 3' splice sites
231 in Col-0. Intriguingly, most of the up-regulated novel 3' splice sites in *xct-1* and *xct-2* were
232 located less than 50 nucleotides downstream of the wild-type 3' splice sites (Fig. 3B;
233 Supplemental Fig. 4A). Studies in human and yeast have demonstrated that the sequences
234 preceding a 3' splice site, including the polypyrimidine tract (PPT) and the pyrimidine at the -3
235 position (Fig. 3A), are important for the strength of the 3' splice site (Horowitz, 2012). Therefore,
236 we further examined the 23-mer sequences flanking the 3' splice sites (from -20 to +3 position).
237 We found that the frequency of the canonical AG sequence at the 3' splice sites was not altered
238 in either *xct-1* or *xct-2* (Fig. 3C; Supplemental Fig. 4B-C). However, the average predicted
239 strength of the 875 down-regulated 3' splice sites in *xct-2* was significantly weaker than the
240 average of total detected 3' splice sites in Col-0 (Fig. 3D). Specifically, the percentage of
241 pyrimidine residues at the -3 position was significantly reduced in down-regulated 3' splice sites
242 compared to that found in all detected 3' splice sites (Fisher's exact test, $P < 0.001$, Fig. 3E),
243 suggesting that functional *XCT* is important for the removal of 3' splice sites with a suboptimal
244 sequence at the -3 position. Moreover, the 532 up-regulated 3' splice sites had an even lower 3'
245 splice site score than the down-regulated sites (Fig. 3D). The frequency of pyrimidines both at
246 the -3 position and throughout the PPT region was significantly lower in the up-regulated

247 junctions (Fig. 3E-F), showing that *xct-2* is less able to discriminate between 3' splice sites
248 during splicing. Taken together, our Iso-Seq data demonstrates that *XCT* controls the accuracy of
249 3' splice site selection, possibly by helping to recognize weaker 3' splice sites and reject sub-
250 optimal downstream sites.
251
252 **The splicing defects of core clock genes are generally more severe in *xct-2* than *xct-1***
253
254 Since aberrant splicing of core clock genes may fully or partially contribute to the altered
255 circadian clock period phenotype in splicing factor mutants (Sanchez et al., 2010; Wang et al.,
256 2012; Jones et al., 2012; Schlaen et al., 2015; Marshall et al., 2016; Li et al., 2019; Feke et al.,
257 2019), we searched for core clock genes with aberrant splicing events in both the short-period
258 *xct-1* and *xct-2* mutants. In total, our Iso-Seq data detected five aberrantly spliced core clock
259 genes, including *LHY*, *LNK2*, *PRR7*, *TOC1* and *TIC* (Fig. 4A). However, we noticed that the
260 ratio of aberrantly-spliced relative to fully-spliced transcripts for several clock genes are
261 significantly higher in *xct-2* than *xct-1*, even though the circadian period defect is more severe in
262 the latter (Supplemental Fig. 5A-D; Supplemental Fig. 1B). We confirmed this finding via semi-
263 qRT-PCR assay (Supplemental Fig. 5E-H). Thus, those results imply that there may be a
264 disconnect between the splicing and circadian clock defects in *xct-1* and *xct-2*.
265
266 **Genes expressed at subjective dawn are enriched among those aberrantly spliced in *xct***
267 **mutants**
268
269 To more broadly explore possible links between the circadian clock and splicing phenotypes in
270 *xct* mutants, we looked for enrichment of circadian clock regulation within genes aberrantly
271 spliced in *xct.* Among the 5,602 previously reported clock-regulated genes (Romanowski et al.,
272 2020) that are detected in our Iso-Seq data, we identified 182 and 402 genes that are mis-spliced
273 in *xct-1* and *xct-2*, respectively (Fig. 4A; Supplemental Dataset 4). However, there is no
274 significant over-representation in either mutant (one-tailed Fisher's exact test, $P = 0.87$ for *xct-1*
275 and 0.99 for *xct-2*), suggesting that *XCT* does not preferentially affect the splicing of clock-
276 regulated genes.
277

278 Previous studies have identified transcripts that are differentially spliced at various times of day
279 (Romanowski et al., 2020; Yang et al., 2020). This suggests that splicing activity may be
280 circadian clock regulated. Therefore, to test whether *XCT* preferentially affects pre-mRNA
281 splicing at certain times of day, we examined the distribution of estimated peak expression times
282 of genes aberrantly spliced in *xct* mutants. We grouped all 5,602 clock-regulated genes into
283 twelve 2-hour intervals based on their estimated peak expression time (Fig. 4B). Genes that are
284 aberrantly spliced in *xct-2* are significantly enriched for peak expression between ZT22 and ZT2
285 compared with the other intervals of the day (Fig. 4C-D, Fisher's exact test, $P < 1e\text{-}4$). Similarly,
286 clock-regulated genes that are aberrantly spliced in *xct-1* also showed a dawn-enriched
287 expression pattern (Supplemental Fig. 6). Collectively, those results indicate that *XCT* activity
288 within the spliceosome may be regulated by the circadian clock.
289
290 To further investigate whether *XCT* preferentially affects splicing of transcripts produced at
291 dawn, we monitored the abundance of candidate splice variants via quantitative reverse
292 transcriptase-polymerase chain reaction (qRT-PCR) over a 24-hour light/dark period (LD)
293 followed by 48 hours in constant light (LL). We selected four circadian-clock-regulated genes
294 and one non-clock-regulated gene that are aberrantly spliced in *xct-2* and fully rescued in *xct-2*
295 *XCT* (Fig. 5A-E). Total transcript levels of clock-regulated genes displayed rhythmic abundance
296 with peak *LHY* and *LNK2* expression at dawn and peak *PRR7* and *TOC1* expression late in the
297 afternoon (Supplemental Fig. 7), as expected (Creux and Harmer, 2019). We found significantly
298 advanced phases of expression in *xct-2* but this mutation did not affect the overall abundance of
299 total transcripts for those genes. However, both the peak and average abundance of the aberrantly
300 spliced isoforms were significantly different in *xct-2* compared with Col-0 (Fig. 5F-J). This
301 serves as validation of the pooling strategy we used to generate our Iso-Seq libraries, where the
302 daily abundance of transcripts was averaged (Fig. 2A; Fig. 5A-E). Contrary to our expectations,
303 instead of preferentially accumulating at dawn, abundance of all splice variants in *xct-2* was
304 synchronized with total transcript levels (Fig. 5F-I; Supplemental Fig. 7). Likewise, the mis-
305 spliced isoform of the non-clock-regulated gene *SPPA* did not show a significant morning peak
306 (Fig. 5J). Meanwhile, the genomic *XCT* complemented line almost completely rescued the
307 splicing defects across the whole experimental period. Taken together, those results suggest that
308 although morning-expressed genes are preferentially enriched among *XCT* targets, *XCT* is

important for the accuracy of pre-mRNA splicing throughout the day under both LD and free-running LL conditions.

Reduction of *PRP19* function rescues the circadian clock but not the splicing defects in *xct-2*

Previous studies revealed that NTC components participate in regulation of circadian clock function in Arabidopsis (Feke et al., 2019; Li et al., 2019). Here we examined circadian period in mutants for several NTC components. We found that mutation in either of the two Arabidopsis *PRP19* homologs, *PRP19A* (*MAC3A*) or *PRP19B* (*MAC3B*), only caused minor lengthening of circadian period. In contrast, the *prp19a-1 prp19b-1* double mutant had a significantly slower circadian clock than Col-0 (Supplemental Fig. 8A), consistent with previously reported redundant roles for *PRP19A* and *PRP19B* in circadian clock regulation (Feke et al., 2019). Similarly, loss of function of other NTC members, including *PRL1*, *CDC5* and *SKIP*, also lengthened the clock period by 1 to 3 hours (Supplemental Fig. 2B; Supplemental Fig. 8B-C), similar to previous reports for *prl1-9* and *skip-1* mutants (Li et al., 2019).

Since *PRP19* co-purifies with *XCT* (Table 1) and they both control the pace of the circadian clock (Supplemental Fig. 8A), we hypothesized they might function in the same pathway to regulate the clock. To test this hypothesis, we introduced *prp19a-1* and *prp19b-1* mutant alleles, which express greatly decreased and near-null levels of *PRP19A* and *PRP19B*, respectively (Supplemental Fig. 9), into the null *xct-2* background and assayed their circadian clock phenotypes. Interestingly, we found that neither the circadian period of *prp19a-1 xct-2* nor of *prp19b-1 xct-2* was significantly different from Col-0 (Fig. 6A; Supplemental Fig. 10), indicating that both *prp19* mutants can fully suppress the short-period phenotype of *xct-2*. Notably, *prp19a-1* and *prp19b-1* single mutants only have slightly longer circadian periods than Col-0. This suggests that the rescued clock function in *prp19 xct* double mutants is not likely due to additive genetic interactions. Thus, our data show that functional *PRP19A* and *PRP19B* are both necessary for *XCT* in regulation of circadian period.

339 To further investigate the functional association between *XCT* and *PRP19*, we next asked
340 whether *prp19* mutants suppress other developmental and physiological defects observed in *xct-2*.
341 In contrast to the circadian period, the reduced rosette size in *xct-2* was not significantly restored
342 in either *prp19a-1 xct-2* or *prp19b-1 xct-2* (Supplemental Fig. 11), indicating that the effects of
343 *XCT* on rosette development and the circadian clock period are genetically separable. This is
344 consistent with our observation that *xct-1* and *xct-2* both have short circadian period phenotypes
345 but only *xct-2* is morphologically different from Col-0 (Supplemental Fig. 1).
346
347 Next, to determine whether suppression of the short clock period phenotype in *xct-2 prp19*
348 mutants is due to reversal of the *xct-2* splicing defects, we conducted qRT-PCR experiments to
349 examine the abundance of *xct*-induced aberrantly-spliced mRNA isoforms of core clock genes in
350 *prp19a-1 xct-2* and *prp19b-1 xct-2*. Surprisingly, none of the aberrantly-spliced isoforms tested
351 showed significantly different abundance in *prp19a-1 xct-2* and *prp19b-1 xct-2* relative to *xct-2*
352 (Fig. 6B-F). Consistent with previous reports for functional redundancy between *PRP19A* and
353 *PRP19B* (Monaghan et al., 2009; Li et al., 2019), we noticed a statistically significant defect in
354 splicing of the third intron of *LNK2* in the *prp19a-1 prp19b-1* double mutant but not the *prp19a-*
355 *1* or *prp19b-1* single mutants. We also checked the expression levels of fully-spliced or total
356 mRNA isoforms of the five core clock genes that are aberrantly-spliced in *xct-2*. In all cases,
357 addition of *prp19a-1* or *prp19b-1* to *xct-2* did not alter the abundance of functionally spliced
358 isoforms of those clock genes (Supplemental Fig. 12). Thus, similar to the developmental defects,
359 the splicing defects of core clock genes are genetically separable from the circadian clock
360 phenotype of *xct-2*.
361
362 **Discussion**
363 The accurate removal of introns from pre-mRNAs is an essential step of gene expression in all
364 eukaryotes. In this work, we report that *XCT* is a global regulator of pre-mRNA splicing in
365 Arabidopsis. Multiple lines of evidence suggest that orthologs of XCT share conserved
366 molecular and cellular functions across kingdoms. Previous mass spectrometry data showed that
367 FAM50A and FAM50B, two human homologs of XCT, physically associate with the affinity-
368 purified spliceosomal C complex (Bessonov et al., 2008; Bessonov et al., 2010). Loss of
369 *FAM50A* function induces transcriptome-wide pre-mRNA splicing defects in both human and

370 zebrafish (Lee et al., 2020). Similarly, a recent study in Arabidopsis also found that XCT
371 associates with spliceosomal proteins and regulates splicing (Liu et al., 2022). In this paper, we
372 show that XCT physically co-purifies with PRP19 and other NTC-associated proteins (Table 1).
373 Furthermore, our PacBio Iso-Seq data indicate that the efficiency and fidelity of pre-mRNA
374 splicing are negatively impacted in both the partial loss-of-function mutant *xct-1* and the null
375 mutant *xct-2* but are largely restored in *xct-2 XCT* (Fig. 2). Therefore, XCT orthologs likely play
376 evolutionarily conserved roles in pre-mRNA splicing. It would be interesting to apply structural
377 biology approaches to further investigate what conserved functional domains among XCT
378 homologs might contribute to their splicing activities.
379
380 Studies have shown that intron retention is the most prevalent type of alternative splicing event
381 in Arabidopsis (Wang and Brendel, 2006; Filichkin et al., 2010). Correspondingly, mutations in
382 many Arabidopsis splicing factors mainly cause intron retention (Supplemental Fig. 3; Schlaen et
383 al., 2015; Li et al., 2019). Here we identify *XCT* as an unusual splicing regulator that specifically
384 controls the fidelity of 3' splice site selection (Fig. 2D-E; Fig. 3). Biochemical studies of splicing
385 in yeast revealed that several DEAH-box ATPases are important for the selection of 3' splice
386 sites (Horowitz, 2012). For example, PRP22, a DEAH-box ATPases that co-purifies with XCT
387 (Table 1; Liu et al., 2022), represses usage of aberrant 3' splice sites and promotes spliceosome
388 scanning for downstream alternative 3' splice sites in yeast (Mayas et al., 2006; Semlow et al.,
389 2016). Studies in human showed that hPRP22, FAM50A and FAM50B, are all abundant in the
390 spliceosomal C complex but nearly absent in B and B* complexes (Bessonov et al., 2008;
391 Bessonov et al., 2010; Zhan et al., 2022). This implies that PRP22 and XCT may have
392 evolutionarily conserved interactions during the second transesterification reaction of splicing,
393 when 5' and 3' splice sites are joined (Fig. 1). Intriguingly, we detected decreased fidelity of 3'
394 splice site selection in both *xct-1* and *xct-2* mutants (Fig. 3; Supplementary Fig. 4), which is also
395 observed in yeast *prp22* mutants (Semlow et al., 2016). Therefore, our results imply that XCT
396 may work with PRP22 to control the fidelity of 3' splice site selection. Future research on the
397 biochemical functions of XCT using *in vitro* and *in vivo* systems could help reveal how it
398 controls splicing fidelity.
399

400 Previous microarray and RNAseq studies demonstrated that transcription and splicing of a large
401 proportion of Arabidopsis genes are under circadian clock regulation (Covington and Harmer,
402 2007; Hsu and Harmer, 2012; Romanowski et al., 2020; Yang et al., 2020). Consequently, timing
403 of sample collection is an important consideration in gene expression and splicing analysis,
404 especially when comparing genotypes with different circadian periods. Here we employed a
405 more efficient sampling method by harvesting plants at twelve evenly distributed time points
406 across a day and pooling them before analysis. Our pooling strategy enabled us to detect
407 transcripts of genes with the distribution of peak phases of expression mirroring that of all clock-
408 regulated genes (Fig. 4B; Romanowski et al., 2020). Overall, this strategy allowed us to identify
409 more clock-regulated differentially spliced transcripts in *xct-2* mutants than in a recent study in
410 which plants were collected at a single time point (Liu et al., 2022). For example, we report
411 novel differential splicing events in afternoon-expressed genes including *PRR7* and *TOC1* (Fig.
412 4A; Supplemental Fig. 7C-D). In fact, our time-course qPCR data suggest that abundance of the
413 aberrantly spliced isoforms of these clock-regulated genes fluctuates by over 99% depending on
414 time of sample collection (Fig. 5F-I). Thus, our results demonstrate the advantages of pooling
415 samples when conducting transcriptome-wide splicing analysis of clock-regulated genes.
416
417 Using this strategy, we were able to investigate whether *XCT* preferentially affects splicing at
418 certain times of day. Indeed, we found that dawn-expressed genes are significantly more likely to
419 be mis-spliced in *xct* mutants than those with other peak phases (Fig. 4C-D; Supplemental Fig. 6).
420 This suggests that *XCT* activity in or its association with the spliceosome may be clock-regulated.
421 An alternative explanation for the overrepresented mis-splicing of dawn-expressed genes could
422 be that *cis*-regulatory elements of those genes might preferentially recruit XCT to control their
423 splicing. This possibility is supported by previous studies showing that XCT orthologs in fission
424 yeast and *Chlamydomonas* are chromatin-associated and in the latter case recruit RNA
425 polymerase II (Pol II) to promoter regions (Anver et al., 2014; Li et al., 2018).
426
427 Alternative splicing regulates various biological processes, including the function of the
428 circadian clock (Hsu and Harmer, 2014; Nolte and Staiger, 2015). In Arabidopsis, such
429 regulation is supported by identification of splicing factor mutants that alter circadian clock
430 period length (Shakhmantsir and Sehgal, 2019). Some splicing factors, such as *GEMIN2* and

431 *SICKLE*, interact epistatically with one or more alternatively spliced clock genes in the control of
432 period length (Schlaen et al., 2015; Marshall et al., 2016), suggesting changes in the pace of the
433 clock are due to altered splicing of these clock genes. Whereas in other cases, the mis-regulated
434 circadian period can only be partially attributed to changes in levels of splicing variants of clock
435 genes (Sanchez et al., 2010; Wang et al., 2012). Additionally, in most splicing factor mutants,
436 only small fractions of total transcripts are aberrantly processed (Jones et al., 2012; Perez-
437 Santángelo et al., 2014; Feke et al., 2019; Li et al., 2019). Therefore, whether these small
438 changes in levels of aberrantly spliced isoforms could lead to significantly decreased levels of
439 functional proteins and thereby cause the observed circadian phenotypes remains unclear.
440
441 Here, we demonstrate that in *xct* mutants the circadian clock phenotype is genetically separable
442 from altered levels of aberrantly spliced mRNA variants of core clock gene. We found that loss
443 of *XCT* function accelerates the clock and causes aberrant splicing of five core clock genes
444 (Supplemental Fig. 1; Fig. 4A). Surprisingly, the clock phenotype but not the splicing defects of
445 the five clock genes in *xct-2* is suppressed by reduction of *PRP19A* or *PRP19B* function (Fig. 6).
446 Similarly, the clock in *xct-1* runs slightly faster than *xct-2* but the splicing defects, including the
447 aberrant splicing of *TOC1*, *TIC* and *CCA1*, are more severe in the latter (Fig. 2; Supplemental
448 Fig. 5). Collectively, these data demonstrate that the short period phenotypes and altered levels
449 of clock gene splicing variants are genetically separable in *xct* mutants.
450
451 How *XCT* regulates the pace of the circadian clock is still an outstanding question. Although we
452 argue that changes in levels of aberrantly spliced clock mRNAs are not responsible for the
453 accelerated clock in *xct* mutants, one possibility is that alterations in the overall kinetics of pre-
454 mRNA splicing may cause circadian period phenotypes. Indeed, pharmacological perturbations
455 of global transcription and translation efficiency can both lengthen the circadian period (de Melo
456 et al., 2021; Uehara et al., 2022). Those results suggest that changes in the kinetics of RNA
457 processing might cause the period phenotypes observed in plants mutated for some splicing
458 factors.
459
460 Alternatively, *XCT* may control the circadian clock function independent of its role in pre-
461 mRNA splicing. In Chlamydomonas, the XCT homolog XAP5 co-immunoprecipitates with

462 RNA Pol II (Li et al., 2018), suggesting that XCT orthologs may possess transcriptional
463 regulatory activities. In this paper, we show that NTC components physically and genetically
464 interact with XCT to regulate circadian clock period (Table 1; Fig. 6A). Besides splicing, another
465 well-characterized role of the NTC in gene expression is regulation of transcriptional elongation
466 (Chanarat and Sträßer, 2013). Studies in both yeast and Arabidopsis have revealed that multiple
467 NTC members, including PRP19, PRL1 and CDC5, physically associate with RNA Pol II and
468 participate in transcript elongation (Chanarat et al., 2011; Zhang et al., 2013; Zhang et al., 2014).
469 In addition, the NTC component SKIP interacts with Polymerase-Associated Factor 1 complex
470 to regulate transcription in a splicing-independent manner (Li et al., 2019). Interestingly, a recent
471 study showed that inhibition of transcriptional elongation by decreasing phosphorylation of the
472 RNA Pol II C-terminal domain lengthens circadian period in Arabidopsis (Uehara et al., 2022). It
473 is therefore possible that *XCT* affects circadian period by altering transcriptional elongation.
474
475 Yet another possibility is that *XCT* affects a cellular process independently of its role in gene
476 expression. For example, PRP19 is known to facilitate DNA repair by its E3 ubiquitin ligase
477 activity independent of its involvement in the spliceosomal complex (Maréchal et al., 2014;
478 Idrissou and Maréchal, 2022). Indeed, there is increasing evidence that many RNA binding
479 proteins directly participate in DNA double-strand break responses (Klaric et al., 2021). A recent
480 study showed that the NTC-associated protein MOS4-ASSOCIATED COMPLEX SUBUNIT
481 5A (MAC5A) physically interacts with the 26S proteasome and regulates its activities in
482 response to DNA damage (Meng et al., 2022). Intriguingly, we recently reported that loss of *XCT*
483 function also disturbs the DNA damage response pathway (Kumimoto et al., 2021). Thus, it is
484 possible that *XCT* works with *PRP19* in this pathway separately from its role in RNA processing.
485 Future research is required to understand the nature of the relationship of between XCT and the
486 NTC in the control of circadian clock function and other essential biological processes.
487
488 **Materials and Methods**
489 **Plant materials and growth conditions**
490
491 All *Arabidopsis thaliana* plants used in this study are Columbia-0 (Col-0) ecotype and contain a
492 *CCR2*::*LUC* reporter for circadian clock assays. The *xct-1*, *xct-2*, *xct-2* p*XCT*::g*XCT-YFP-HA*,

493 *prp19a-1*, *prp19b-1*, *prl1-2*, *cdc5-1* and *skip-1* genotypes have been previously described
494 (Martin-Tryon and Harmer, 2008; Monaghan et al., 2009; Zhang et al., 2014; Wang et al., 2012).
495 All the double mutants in this study were produced by crossing. Unless otherwise specified,
496 seeds were surface sterilized with chlorine gas for 3 hours (50 ml 100% bleach + 3ml 1M HCl)
497 and then plated on 1x Murashige and Skoog (MS) growth media containing 0.7% agar, pH 5.7.
498 After 3d stratification in dark at 4˚C, plates were transferred to 12-h light (cool white fluorescent
499 bulbs, 55 µmol m^{-2} s^{-1}) / 12-h dark cycles at 22˚C for a variable number of days depending on the
500 experiment.
501
502 **Immunoprecipitations and mass spectrometry**
503
504 Plants were grown in 12-h light / 12-h dark cycles and harvested on day 10 at ZT3 or ZT17.
505 Approximately 7.5g of vegetative tissue was flash frozen in liquid nitrogen and ground into fine
506 powder with a mortar and pestle. Ground tissue was resuspended in nuclei enrichment buffer (50
507 mM Tris pH7.5, 400 mM sucrose, 2.5 mM $MgCl_2$, 1 mM DTT, 1 mM PMSF, cOmplete Protease
508 Inhibitor cocktail (Roche)), the nuclear pellet was collected, resuspended in IP buffer (100mM
509 Tris pH7.5, 1mM EDTA, 75mM NaCl, 10% glycerol, 0.3% Triton X-100, 0.05% SDS, 10 mM
510 MG-132, 1 mM PMSF, , cOmplete Protease Inhibitor cocktail (Roche)) and pelleted again.
511 Nuclei were resuspended in IP buffer, disrupted via sonication, and adjusted to 1 mg/mL in IP
512 buffer. 1 mg of extract was incubated with µMACS MicroBeads conjugated to an anti-HA
513 monoclonal antibody (Miltenyi Biotec) and beads were then captured on µMACS M-colums.
514 Beads were washed 3x with ice cold IP buffer and 1x with ice cold TE buffer (10 mM Tris-HCl
515 pH 8.0, 0.1 mM EDTA). Proteins were eluted off the beads with elution buffer (Miltenyi Biotec).
516 Proteins were resolved using SDS polyacrylamide gel electrophoresis and gels were sent to the
517 Rutgers Biological Mass Spectrometry Facility, Robert Wood Johnson Medical School. Proteins
518 were eluted and subjected to mass spectrometry as previously described (Wei et al., 2020).
519
520 **PacBio Iso-Seq and bioinformatic analysis**
521
522 Arabidopsis seeds were surface sterilized in 70% ethanol prepared in 0.1% (v/v) Triton X-100
523 (Sigma) for 5 minutes and then in 100% Ethanol for 20 minutes. After air drying, seeds were

524 plated on 1x MS growth media containing 0.7% agar. After cold stratification for 3 days, plates
525 were transferred to constant light (55 µmol m^{-2} s^{-1}) and temperature (22˚C). Approximately 60
526 mg of whole seedlings of each genotype were collected every 2h over 24 hours on day 11 and
527 pooled as indicated in Fig. 2A. Three biological replicates were collected for each genotype.
528 Samples were flash-frozen in liquid nitrogen, and ground into fine powder using a beadbeater.
529 Total RNA was extracted using an RNeasy Plant Mini Kit (Qiagen) followed by purification
530 using the RNA Clean & Concentrator Kit (Zymo Research). Purified RNAs were quantified
531 using a Nanodrop (ThermoFisher) and quality control was performed by an Agilent Bioanalyzer
532 2100. All samples had a 260/230 nm ratio higher than 1.9, 260/280nm ratio between 2 and 2.15,
533 and RIN score higher than 8. PacBio Sequel II library preparation and RNA-sequencing (Iso-Seq)
534 was performed by UC Davis DNA Technologies & Expression Analysis Core
535 (https://dnatech.genomecenter.ucdavis.edu/pacbio-library-prep-sequencing/).
536
537 Raw reads generated by the PacBio Sequel II sequencer were imported into PacBio SMRT Link
538 v 8.0 for Circular Consensus Sequence (CCS) calling and demultiplexing. Next, poly(A) tails
539 and concatemers were removed using the refine command from isoseq3 package via Bioconda (v
540 3.10) with the option '--require-polya'. Then the fastq files containing full-length non-
541 concatemer reads were mapped to Arabidopsis TAIR 10 genome assembly using minimap2 (v
542 2.17) with the parameter '-ax splice -t 30 -uf --secondary=no -C5'. For differential splicing
543 analysis, counts of exonic regions and known/novel splice junctions were generated using
544 QoRTs software package (v 1.3.6) (Hartley and Mullikin, 2015) with the parameter '--stranded --
545 singleEnded --stranded_fr_secondstrand --keepMultiMapped'. To adapt to the long-read data,
546 the 'maxPhredScore' was set to 93 and the 'maxReadLength' was adjusted manually for each
547 library. To increase the power of detecting novel splice junctions, the '--minCount' threshold was
548 set to 5. The raw count data was then loaded to JunctionSeq R package (v 1.5.4) (Hartley and
549 Mullikin, 2016) to determine differential usage of exons or splice junctions relative to the overall
550 expression of the corresponding gene with a false discovery rate (FDR) of 0.05. Genes with at
551 least one differentially spliced exon/junction were compared to the total circadian-clock-
552 regulated genes (Romanowski et al., 2020) as described in Fig. 4.
553
554 **RNA extraction and RT-PCR**

555

556 For time-course qRT-PCR analysis, Arabidopsis seedlings were entrained in 12-h light / 12-h
557 dark cycles for 9 days before transferred to constant light and temperature (55 µmol m^{-2} s^{-1},
558 22˚C). Starting from day 9, approximately 15-20 whole seedlings of each genotype were
559 harvested every 4h over the 72-h period. For single time point gene expression and splicing
560 analysis, 10-d-old seedlings grown in 12-h light / 12-h dark cycles at 22˚C were harvested at
561 estimated peak time of expression for each studied gene. Collected tissue was immediately
562 frozen in liquid nitrogen and ground into fine powder using a beadbeater. Total RNA was
563 isolated using TRIzol reagent (Invitrogen) and quantified with a Nanodrop (ThermoFisher). 200
564 ng of total RNA was used for cDNA synthesis with an oligo(dT)18 primer and SuperScriptIII
565 (Invitrogen) reverse transcriptase. Diluted cDNAs were used as templates for qRT-PCR and
566 semi-qRT-PCR reactions. The qRT-PCR was carried out as previously described (Martin-Tryon
567 et al., 2007) using a Bio-Rad CFX96 thermocycler. Primers amplifying the aberrantly spliced or
568 total transcripts were tested by standard curve and melt curve assays. Relative expression (ΔΔCq)
569 values were normalized to the geometric mean of *PROTEIN PHOSPHATASE 2a* (*PP2A*) and
570 *ISOPENTENYL DIPHOSPHATE ISOMERASE 2* (*IPP2*) expression levels. For semi-qRT-PCR,
571 splice-junction specific primer pairs were designed to amplify regions flanking the aberrantly
572 spliced introns of interest. The size and abundance of the resultant PCR products were then
573 analyzed and quantified by LabChip GX bioanalyzer (PerkinElmer). The expression analyses
574 represent two to three biological replicates. All primers used in this study are described in
575 Supplemental Dataset 5.

576

577 **Circadian period analysis**

578

579 After growing on MS plates under 12-h light / 12-h dark cycles for 6 days, Arabidopsis seedlings
580 were sprayed with 3 mM D-luciferin (Biosynth) prepared in 0.01% (v/v) Triton X-100 (Sigma)
581 and then transferred to a growth chamber with a constant 22˚C and constant light provided by red
582 and blue LED SnapLites (Quantum Devices, 35 µmol m^{-2} s^{-1} each) for imaging. Luciferase
583 activity was detected using a cooled CCD camera (DU434-BV [Andor Technology]).
584 Bioluminescence signals from the images were quantified using MetaMorph 7.7.1.0 software
585 (Molecular Devices). Subsequent circadian period estimation and rhythmicity analysis were

586 performed using Biological Rhythms Analysis Software System 3.0 (BRASS) by fitting the
587 bioluminescence data to a cosine wave through Fourier Fast Transform-Non-Linear Least
588 Squares (Plautz et al., 1997).
589
590 **Rosette size measurement**
591
592 Seeds on MS plates were germinated in a growth chamber with 12-h light / 12-h dark cycles at a
593 constant 22˚C. 15-day-old seedlings were transferred to soil and grown in 16-h light (cool-white
594 fluorescent bulbs, 75 µmol m^{-2} s^{-1}) / 8-h dark long day condition at a constant 22˚C. Rosette sizes
595 of 39-day-old plants were determined by the greatest distance between rosette leaves using a
596 digital caliper.
597
598 **Accession Numbers**
599
600 All the *Arabidopsis thaliana* genes studied in this paper can be found under the following
601 accession numbers:
602 *XCT*, AT2G21150
603 *PRP19A*, AT1G04510
604 *PRP19B*, AT2G33340
605 *PRL1*, AT4G15900
606 *SKIP*, AT1G77180
607 *CDC5*, AT1G09770
608 *LHY*, AT1G01060
609 *LNK2*, AT3G54500
610 *TIC*, AT3G22380
611 *PRR7*, AT5G02810
612 *TOC1*, AT5G61380
613 *SPPA*, AT1G73990
614 *IPP2*, AT3G02780
615 *PP2A*, AT1G69960
616 *CCA1*, AT2G46830

617

618 **Data Availability**

619

620 All our MS data were deposited and available at Center for Computational Mass Spectrometry
621 (CCMS, Dataset: MSV000090830). Our PacBio Iso-Seq data were deposited and available in
622 NCBI Gene Expression Omnibus (GEO, Accession number: GSE220902).

623

624 **Funding**

625

626 This work was supported by awards from the National Institutes of Health (R01 GM069418 to
627 SLH) and the United States Department of Agriculture-National Institute of Food and
628 Agriculture (CA-D-PLB-2259-H to SLH). HZ was supported by a fellowship from China
629 Scholarship Council (CSC #201806010204 to HZ).

630

631 **Acknowledgments**

632

633 We thank the Arabidopsis Biological Resource Center for providing seeds. We thank Haiyan
634 Zheng and the Biological Mass Spectrometry Facility of Robert Wood Johnson Medical School
635 and Rutgers for mass spectrometry analysis. They are supported by NIH Shared Instrumentation
636 Grant S10OD01640. We thank the DNA Technologies and Expression Analysis Core at the UC
637 Davis Genome Center for performing PacBio Iso-Seq experiment. They are supported by NIH
638 Shared Instrumentation Grant 1S10OD010786-01. We thank Julin Maloof for statistical advice,
639 as well as members of the Harmer, Maloof, and Shabek labs for helpful discussions.

640

641 **Author Contributions**

642

643 HZ, RWK and SLH designed the research; HZ, RWK, and SA performed the research; HZ,
644 RWK, and SLH analyzed data; HZ and SLH wrote the paper.

645

646 **Figure Legends**

647

648 **Figure 1. Simplified overview of pre-mRNA splicing reactions.** A schematic diagram
649 highlighting the two catalytic transesterification steps and the association between the NTC and
650 the spliceosomal complex during pre-mRNA splicing. Gray boxes and solid black lines represent
651 exons and introns, respectively. U1-U6 small nuclear ribonucleoproteins (snRNPs) are indicated
652 by yellow circles. The NTC is indicated by a green oval.
653
654 **Figure 2. Transcriptome-wide analysis reveals *XCT* as a global pre-mRNA splicing**
655 **regulator.** A, Experimental design and sampling method for the PacBio Iso-Seq experiment.
656 White and grey boxes represent subjective day and subjective night, respectively. Arabidopsis
657 seedlings were grown at constant light and temperature for 10 days before being harvested and
658 pooled. B and C, Numbers of differentially enriched splicing events represented by significantly
659 differentially down- (B) or up-regulated (C) splice junctions in *xct-1*, *xct-2* and *xct-2*
660 complemented with p*XCT*::g*XCT-YFP-HA* compared with Col-0 (false discovery rate < 0.05). D
661 and E, Frequency of different classes of 5' and 3' splice sites among down- (D) or up-regulated
662 (E) splice junctions in *xct-1* and *xct-2*. Known or novel splice sites were classified by comparing
663 to TAIR10 genome annotation.
664
665 **Figure 3. *XCT* is required for the fidelity of 3' splice site selection during pre-mRNA**
666 **splicing.** A, A schematic diagram showing the structure of a typical U2-type splice junction. Y:
667 pyrimidine. B, Distribution of the distance between each pair of novel 3' splice site and its
668 corresponding canonical 3' splice sites in *xct-2*. C, Pictograms showing the frequency of
669 nucleotides in the 23-mers sequences flanking the 3' splice sites in all expressed, down-regulated
670 and up-regulated splice junctions in *xct-2*. D, Maximum Entropy Model scores showing the
671 strength of 3' splice sites of all expressed, down-regulated and up-regulated junctions in *xct-2*. E,
672 Percentage of pyrimidines at the -3 position (i.e. the nucleotide preceding the AG at 3' splice
673 site) in *xct-2*. F, Counts of pyrimidines in the Y10 polypyrimidine tract upstream of the 3' splice
674 sites in *xct-2*. PPT, polypyrimidine tract. The lines in the boxplot represent the 75% quartile,
675 median and 25% quartile of the data, respectively. Statistical significance in (D) and (F) was
676 determined using linear regression model with junction class as a fixed effect and is shown in
677 lower case letters (Tukey's multiple comparison test, $P < 0.05$). Statistical significance in (E) was
678 determined by Fisher's exact test: **: $P < 0.01$; ***: $P < 0.001$.

679

680 **Figure 4. Dawn-phased genes are significantly enriched among all the circadian-clock-**
681 **regulated genes that are aberrantly spliced in *xct-2.*** A, Venn diagram showing the overlaps of
682 aberrantly spliced genes in *xct-1, xct-2*, and total circadian-clock-regulated genes (Romanowski
683 et al., 2020). The core circadian clock genes that are mis-spliced in both *xct* mutants are indicated
684 in red (non-clock-regulated) and blue (clock-regulated) fonts. Only genes considered as
685 'detected' in all three RNA-Seq datasets are included. B and C, Phases of estimated peak
686 expression of all circadian clock-regulated genes (Romanowski et al., 2020) that are detected (B)
687 or significantly aberrantly spliced (C) in *xct-2*. The white and gray backgrounds represent the
688 subjective day and subjective night, respectively. D, Distribution of *P*-values from Fisher's extact
689 tests calculating whether the ratio of the number of aberrantly spliced genes in (B) to total clock-
690 regulated genes in (A) is significantly higher than expected by chance in each 2-hour interval.

691

692 **Figure 5. Time-course qRT-PCR experiments validate the role of *XCT* in regulating pre-**
693 **mRNA splicing of clock-regulated and non-clock-regulated genes.** A - E, Sashimi plots
694 showing PacBio Iso-Seq reads mapped to *LHY* (A)*, LNK2* (B)*, PRR7* (C)*, TOC1* (D) and *SPPA*
695 (E) in Col-0 (teal)*, xct-2* (orange) and *xct-2 XCT* (purple). The red rectangles highlight the
696 aberrantly spliced exon-exon junctions that are examined by qRT-PCR in (F) - (J). F - J,
697 Normalized expression of the aberrantly spliced isoforms of *LHY* (F)*, LNK2* (G)*, PRR7* (H)*,*
698 *TOC1* (I) and *SPPA* (J) in Col-0*, xct-2* and *xct-2 XCT*. Samples were collected every four hours
699 over a 72-h window. Expression levels were examined by qRT-PCR using splice-junction-
700 specific primers and normalized to *PP2*A and *IPP2.* Data points represent mean ± se from three
701 independent biological replicates. For each isoform in each biological replicate, the normalized
702 expression levels were relative to the highest expression levels of their total transcripts in Col-0
703 across all time points. Teal lines, wild type Col-0; orange lines, *xct-2* mutants; purple lines, *xct-2*
704 *XCT*. Black background, dark period; white and gray background, light period during subjective
705 day and night, respectively.

706

707 **Figure 6. Loss of *PRP19* function suppresses the short circadian clock period phenotype**
708 **but not the splicing defects of core clock genes in *xct-2*.** A, Circadian periods of Col-0, *xct-2*,
709 *prp19a-1*, *prp19b-1*, *prp19a-1 prp19b-1*, *prp19a-1 xct-2* and *prp19b-1 xct-2* plants. B - F,

710 Normalized expression of the aberrantly spliced isoforms of *LHY, LNK2, TIC, PRR7* and *TOC1*
711 in Col-0, *xct-2*, *prp19a-1*, *prp19b-1*, *prp19a-1 prp19b-1*, *prp19a-1 xct-2* and *prp19b-1 xct-2*.
712 Samples were collected at the estimated peak expression time for each gene. Expression levels
713 were examined by qRT-PCR using splice-junction-specific primers and normalized to *PP2*A and
714 *IPP2.* Data points represent mean ± se from two independent biological replicates. Statistical
715 significance was determined using linear regression model with genotype as a fixed effect and is
716 shown in lower case letters (Tukey's multiple comparison test, $P < 0.05$).
717
718 **Table 1. XCT physically associates with splicing-related proteins, especially the NTC**
719 **components, in Arabidopsis.** Mass Spectrometry (MS) data showing that spliceosome-
720 associated proteins are significantly more enriched in XCT-YFP-HA-IP than control IP (fold
721 enrichment > 3; *P*-value < 0.05, Welch two sample t.test). The full list of proteins co-purified
722 with XCT are described in Supplemental Dataset 1. Only proteins detected in each biological
723 replicate and with 20 or more total peptides counts are shown.
724
725 **Supplemental Materials**
726
727 **Supplemental Figure 1. *XCT* regulates plant development and the pace of the circadian**
728 **clock in *Arabidopsis thaliana.*** A, Morphology of 52-day-old Col-0, *xct-1*, *xct-2* mutant plants
729 and *xct-2* complemented with p*XCT*::g*XCT-YFP-HA.* Bar = 10 mm. B, Circadian periods of
730 genotypes described in (A). The lines in the boxplot represent the 75% quartile, median and 25%
731 quartile of the data, respectively. Statistical significance was determined using linear regression
732 model with genotype as a fixed effect and is shown in lower case letters (Tukey's multiple
733 comparison test, $P < 0.05$).
734
735 **Supplemental Figure 2. *XCT* and *PRL1* control the pace of the circadian clock in an**
736 **opposite manner.** A, Morphology of 21-day-old Col-0, *xct-1*, *xct-2* and *prl1-2* mutant
737 Arabidopsis seedlings. Bar = 1 mm. B, Circadian clock periods of plant genotypes described in
738 (A). The lines in the boxplot represent the 75% quartile, median and 25% quartile of the data,
739 respectively. Statistical significance was determined using linear regression model with genotype
740 as a fixed effect and is shown in lower case letters (Tukey's multiple comparison test, $P < 0.05$).

741

742 **Supplemental Figure 3. *prl1-2* mutant mainly induces intron retention defects in**
743 **Arabidopsis.** Frequency of different classes of 5' and 3' splice sites of down- (teal) or up-
744 regulated (orange) junctions in *prl1-2* compared to wild type. Known or novel splice sites were
745 classified based on TAIR10 genome annotation.

746

747 **Supplemental Figure 4. *xct-1* mutant displays reduced fidelity of 3' splice site selection**
748 **during pre-mRNA splicing.** A, Distribution of the distances between each mis-selected novel 3'
749 splice site and its corresponding canonical 3' splice site in *xct-1*. B - C, Pictograms showing the
750 frequency of nucleotides in the 23-mers sequences flanking the 3' splice sites in splice junctions
751 that are down-regulated or up-regulated in *xct-1*.

752

753 **Supplemental Figure 5. The splicing defects of core clock genes are more severe in *xct-2***
754 **than *xct-1*.** A - D, Sashimi plots showing PacBio Iso-Seq reads mapped to *CCA1* (A), *LNK2* (B),
755 *TOC1* (C) and *TIC* (D) in Col-0 (teal), *xct-1* (yellow) and *xct-2* (orange). The red rectangles
756 highlight the aberrantly spliced exon-exon junctions that are examined by semi-qRT-PCR in (E)
757 - (H). E - H, Relative abundance of aberrantly-spliced to fully-spliced isoforms of *CCA1* (E),
758 *LNK2* (F), *TOC1* (G) and *TIC* (H). Differentially spliced isoforms were amplified by semi-qRT-
759 PCR using primers flanking the examined regions, followed by separation and quantification
760 using a Lab Chip GX bioanalyzer. Statistical significance was determined using linear regression
761 models with genotype as a fixed effect and is shown in lower case letters (Tukey's multiple
762 comparison test, $P < 0.05$).

763

764 **Supplemental Figure 6. Dawn-phased genes are significantly enriched among genes mis-**
765 **spliced in *xct-1*.** A - B, Phases of peak expression of all the circadian-clock-regulated genes
766 (Romanowski et al., 2020) that are detected (A) or aberrantly spliced (B) in *xct-1*. The white and
767 gray backgrounds represent the subjective day and subjective night, respectively. C, Distribution
768 of *P*-values from Fisher's exact test calculating whether the ratio of the number of mis-spliced
769 genes in (B) to all clock-regulated genes in (A) is significantly higher than expected by chance
770 for each 2-hour interval.

771

772 **Supplemental Figure 7. Loss of *XCT* function does not affect overall abundance of**
773 **transcripts of core-circadian-clock genes that are aberrantly spliced in *xct* mutants.** A - F,
774 Normalized expression of the total transcript levels of *LHY* (A)*, LNK2* (B), *PRR7* (C) and *TOC1*
775 (D) in Col-0*, xct-2* and *xct-2 XCT*. Samples were collected every four hours over a 72-h window.
776 Expression levels were examined by qRT-PCR using primers that detect abundance of all
777 transcripts and normalized to *PP2*A and *IPP2.* Data points represent mean ± se from three
778 independent biological replicates. For each isoform in each biological replicate, the normalized
779 expression levels were relative to the highest expression level in Col-0 across all time points.
780 Teal lines, wild type Col-0; orange lines, *xct-2* muants; purple lines, *xct-2* complemented with
781 p*XCT*::g*XCT-YFP-HA*. Black background, dark period; white and gray background, light period
782 during subjective day and night, respectively.
783
784 **Supplemental Figure 8. Mutation of Arabidopsis NTC members lengthens circadian**
785 **period.** A - C, Circadian periods of Col-0 and NTC mutant plants, including (A) *prp19a-1*,
786 *prp19b-1*, *prp19a-1 prp19b-1*, (B) *cdc5-1*, and (C) *skip-1*. The lines in the boxplot represent the
787 75% quartile, median and 25% quartile of the data, respectively. Statistical significance was
788 determined using linear regression model with genotype as a fixed effect and is shown in lower
789 case letters (Tukey's multiple comparison test, $P < 0.05$).
790
791 **Supplemental Figure 9. *PRP19A* (*MAC3A*) and *PRP19B* (*MAC3B*) transcript levels are**
792 **highly reduced in *prp19a-1* and *prp19b-1* mutant backgrounds, respectively.** A - B,
793 Normalized expression of (A) *PRP19A* and (B) *PRP19B* in Col-0, *xct-2*, *prp19a-1*, *prp19b-1*,
794 *prp19a-1 prp19b-1*, *prp19a-1 xct-2* and *prp19b-1 xct-2*. Expression levels were examined by
795 qRT-PCR and normalized to *PP2*A and *IPP2.* Data points represent mean ± se from two
796 independent biological replicates. Samples were collected at ZT0. Statistical significance was
797 determined using linear regression model with genotype as a fixed effect and is shown in lower
798 case letters (Tukey's multiple comparison test, $P < 0.05$).
799
800 **Supplemental Figure 10. Loss of *PRP19* function suppresses the *xct-2* short circadian**
801 **period phenotype.** An independent replicate of the experiment in Figure 6A showing the

802 circadian periods of Col-0, *xct-2*, *prp19a-1*, *prp19b-1*, *prp19a-1 prp19b-1*, *prp19a-1 xct-2* and
803 *prp19b-1 xct-2* plants.
804
805 **Supplemental Figure 11. *PRP19* and *XCT* additively regulate Arabidopsis rosette size.** A,
806 Morphology of 39-day-old Col-0, *xct-2*, *prp19a-1*, *prp19b-1*, *prp19a-1 prp19b-1*, *prp19b-1 xct-2*
807 and *prp19a-1 xct-2* plants. Bar = 10 mm. B, Rosette diameter of 36-day-old plants grown under
808 long-day conditions at 22˚C (n = 5-11). Data are shown as mean ± se. Statistical significance was
809 determined using linear regression model with genotype as a fixed effect and is shown in lower
810 case letters (Tukey's multiple comparison test, $P < 0.05$).
811
812 **Supplemental Figure 12. Levels of total transcripts of *XCT*-targeted core clock genes are**
813 **not altered in *prp19a-1 xct-2* or *prp19b-1 xct-2* compared to *xct-2.*** A - F, Normalized
814 expression of total transcript levels (A, C, E, F) or specific normally spliced isoforms (B, D) of
815 *LHY, LNK2, TIC, PRR7* and *TOC1* in Col-0, *xct-2*, *prp19a-1*, *prp19b-1*, *prp19a-1 prp19b-1*,
816 *prp19a-1 xct-2* and *prp19b-1 xct-2*. Expression levels were examined by qRT-PCR using primers
817 that detect abundance of all transcripts or normally spliced isoforms and normalized to *PP2*A and
818 *IPP2.* Data points represent mean ± se from two independent biological replicates. Samples were
819 collected at the estimated peak expression time for each gene. Statistical significance was
820 determined using linear regression model with genotype as a fixed effect and is shown in lower
821 case letters (Tukey's multiple comparison test, $P < 0.05$).
822
823 **Supplemental Dataset 1. A list of proteins co-purified with XCT-IP detected by MS.**
824
825 **Supplemental Dataset 2. Summary of full-length reads obtained from each PacBio Iso-Seq**
826 **library.**
827
828 **Supplemental Dataset 3. Lists of significant differential splicing events identified by**
829 **JunctionSeq.**
830
831 **Supplemental Dataset 4. Lists of total and aberrantly spliced circadian-clock-regulated**
832 **genes described in this study.**

833

834 **Supplemental Dataset 5. A list of primers used in this study.**

835

836 **References**

837

838 **Anver S, Roguev A, Zofall M, Krogan NJ, Grewal SIS, Harmer SL** (2014) Yeast X-
839 chromosome-associated protein 5 (Xap5) functions with H2A.Z to suppress aberrant
840 transcripts. EMBO Rep **15**: 894–902

841 **Bessonov S, Anokhina M, Krasauskas A, Golas MM, Sander B, Will CL, Urlaub H, Stark**
842 **H, Lührmann R** (2010) Characterization of purified human Bact spliceosomal
843 complexes reveals compositional and morphological changes during spliceosome
844 activation and first step catalysis. RNA **16**: 2384–2403

845 **Bessonov S, Anokhina M, Will CL, Urlaub H, Lührmann R** (2008) Isolation of an active step
846 I spliceosome and composition of its RNP core. Nature **452**: 846–850

847 **Chanarat S, Seizl M, Strässer K** (2011) The Prp19 complex is a novel transcription elongation
848 factor required for TREX occupancy at transcribed genes. Genes Dev **25**: 1147–1158

849 **Chanarat S, Sträßer K** (2013) Splicing and beyond: the many faces of the Prp19 complex.
850 Biochim Biophys Acta **1833**: 2126–2134

851 **Clough SJ, Bent AF** (1998) Floral dip: a simplified method for Agrobacterium-mediated
852 transformation of Arabidopsis thaliana. Plant J **16**: 735–743

853 **Covington MF, Harmer SL** (2007) The circadian clock regulates auxin signaling and responses
854 in Arabidopsis. PLoS Biol **5**: e222

855 **Creux N, Harmer S** (2019) Circadian Rhythms in Plants. Cold Spring Harb Perspect Biol **11**:
856 a034611

857 **Deng X, Lu T, Wang L, Gu L, Sun J, Kong X, Liu C, Cao X** (2016) Recruitment of the
858 NineTeen Complex to the activated spliceosome requires AtPRMT5. Proc Natl Acad Sci
859 U S A **113**: 5447–5452

860 **Fang X, Shi Y, Lu X, Chen Z, Qi Y** (2015) CMA33/XCT Regulates Small RNA Production
861 through Modulating the Transcription of Dicer-Like Genes in Arabidopsis. Mol Plant **8**:
862 1227–1236

863 **Feke A, Liu W, Hong J, Li M-W, Lee C-M, Zhou EK, Gendron JM** (2019) Decoys provide a
864 scalable platform for the identification of plant E3 ubiquitin ligases that regulate
865 circadian function. Elife **8**: e44558

866 **Filichkin SA, Priest HD, Givan SA, Shen R, Bryant DW, Fox SE, Wong W-K, Mockler TC**
867 (2010) Genome-wide mapping of alternative splicing in Arabidopsis thaliana. Genome
868 Res **20**: 45–58

869 **Harmer SL** (2009) The circadian system in higher plants. Annu Rev Plant Biol **60**: 357–377

870 **Hartley SW, Mullikin JC** (2016) Detection and visualization of differential splicing in RNA-
871 Seq data with JunctionSeq. Nucleic Acids Res **44**: e127

872 **Hartley SW, Mullikin JC** (2015) QoRTs: a comprehensive toolset for quality control and data
873 processing of RNA-Seq experiments. BMC Bioinformatics **16**: 224

874 **Hatakeyama S, Yada M, Matsumoto M, Ishida N, Nakayama KI** (2001) U box proteins as a
875 new family of ubiquitin-protein ligases. J Biol Chem **276**: 33111–33120

876 **Hogg R, McGrail JC, O'Keefe RT** (2010) The function of the NineTeen Complex (NTC) in
877 regulating spliceosome conformations and fidelity during pre-mRNA splicing. Biochem
878 Soc Trans **38**: 1110–1115

879 **Horowitz DS** (2012) The mechanism of the second step of pre-mRNA splicing. Wiley
880 Interdiscip Rev RNA **3**: 331–350

881 **Hsu PY, Harmer SL** (2012) Circadian phase has profound effects on differential expression
882 analysis. PLoS One **7**: e49853

883 **Hsu PY, Harmer SL** (2014) Wheels within wheels: the plant circadian system. Trends Plant Sci
884 **19**: 240–249

885 **Idrissou M, Maréchal A** (2022) The PRP19 Ubiquitin Ligase, Standing at the Cross-Roads of
886 mRNA Processing and Genome Stability. Cancers (Basel) **14**: 878

887 **James AB, Syed NH, Bordage S, Marshall J, Nimmo GA, Jenkins GI, Herzyk P, Brown**
888 **JWS, Nimmo HG** (2012) Alternative splicing mediates responses of the Arabidopsis
889 circadian clock to temperature changes. Plant Cell **24**: 961–981

890 **Jia T, Zhang B, You C, Zhang Y, Zeng L, Li S, Johnson KCM, Yu B, Li X, Chen X** (2017)
891 The Arabidopsis MOS4-Associated Complex Promotes MicroRNA Biogenesis and
892 Precursor Messenger RNA Splicing. Plant Cell **29**: 2626–2643

893 **Jones MA, Williams BA, McNicol J, Simpson CG, Brown JWS, Harmer SL** (2012) Mutation
894 of Arabidopsis spliceosomal timekeeper locus1 causes circadian clock defects. Plant Cell
895 **24**: 4066–4082

896 **Klaric JA, Wüst S, Panier S** (2021) New Faces of old Friends: Emerging new Roles of RNA-
897 Binding Proteins in the DNA Double-Strand Break Response. Front Mol Biosci **8**:
898 668821

899 **Koncz C, Dejong F, Villacorta N, Szakonyi D, Koncz Z** (2012) The spliceosome-activating
900 complex: molecular mechanisms underlying the function of a pleiotropic regulator. Front
901 Plant Sci **3**: 9

902 **Kumimoto RW, Ellison CT, Toruño TY, Bak A, Zhang H, Casteel CL, Coaker G, Harmer**
903 **SL** (2021) XAP5 CIRCADIAN TIMEKEEPER Affects Both DNA Damage Responses
904 and Immune Signaling in Arabidopsis. Front Plant Sci **12**: 707923

905 **Kwon Y-J, Park M-J, Kim S-G, Baldwin IT, Park C-M** (2014) Alternative splicing and
906 nonsense-mediated decay of circadian clock genes under environmental stress conditions
907 in Arabidopsis. BMC Plant Biol **14**: 136

908 **Lee Y-R, Khan K, Armfield-Uhas K, Srikanth S, Thompson NA, Pardo M, Yu L, Norris**
909 **JW, Peng Y, Gripp KW, et al** (2020) Mutations in FAM50A suggest that Armfield
910 XLID syndrome is a spliceosomopathy. Nat Commun **11**: 3698

911 **Li L, Tian G, Peng H, Meng D, Wang L, Hu X, Tian C, He M, Zhou J, Chen L, et al** (2018)
912 New class of transcription factors controls flagellar assembly by recruiting RNA
913 polymerase II in Chlamydomonas. Proc Natl Acad Sci U S A **115**: 4435–4440

914 **Li Y, Yang J, Shang X, Lv W, Xia C, Wang C, Feng J, Cao Y, He H, Li L, et al** (2019) SKIP
915 regulates environmental fitness and floral transition by forming two distinct complexes in
916 Arabidopsis. New Phytol **224**: 321–335

917 **Liu L, Li X, Yuan L, Zhang G, Gao H, Xu X, Zhao H** (2022) XAP5 CIRCADIAN
918 TIMEKEEPER specifically modulates 3' splice site recognition and is important for
919 circadian clock regulation partly by alternative splicing of LHY and TIC. Plant Physiol
920 Biochem **172**: 151–157

921 **Maréchal A, Li J-M, Ji XY, Wu C-S, Yazinski SA, Nguyen HD, Liu S, Jiménez AE, Jin J,**
922 **Zou L** (2014) PRP19 transforms into a sensor of RPA-ssDNA after DNA damage and
923 drives ATR activation via a ubiquitin-mediated circuitry. Mol Cell **53**: 235–246

924 **Marshall CM, Tartaglio V, Duarte M, Harmon FG** (2016) The Arabidopsis sickle Mutant
925 Exhibits Altered Circadian Clock Responses to Cool Temperatures and Temperature-
926 Dependent Alternative Splicing. Plant Cell **28**: 2560–2575

927 **Martin-Tryon EL, Harmer SL** (2008) XAP5 CIRCADIAN TIMEKEEPER coordinates light
928 signals for proper timing of photomorphogenesis and the circadian clock in Arabidopsis.
929 Plant Cell **20**: 1244–1259

930 **Martin-Tryon EL, Kreps JA, Harmer SL** (2007) GIGANTEA acts in blue light signaling and
931 has biochemically separable roles in circadian clock and flowering time regulation. Plant
932 Physiol **143**: 473–486

933 **Mayas RM, Maita H, Staley JP** (2006) Exon ligation is proofread by the DExD/H-box ATPase
934 Prp22p. Nat Struct Mol Biol **13**: 482–490

935 **de Melo JRF, Gutsch A, Caluwé TD, Leloup J-C, Gonze D, Hermans C, Webb AAR,**
936 **Verbruggen N** (2021) Magnesium maintains the length of the circadian period in
937 Arabidopsis. Plant Physiol **185**: 519–532

938 **Meng X, Wang Q, Hao R, Li X, Li M, Hu R, Du H, Hu Z, Yu B, Li S** (2022) RNA-binding
939 protein MAC5A interacts with the 26S proteasome to regulate DNA damage response in
940 Arabidopsis. Plant Physiol kiac510

941 **Monaghan J, Xu F, Gao M, Zhao Q, Palma K, Long C, Chen S, Zhang Y, Li X** (2009) Two
942 Prp19-like U-box proteins in the MOS4-associated complex play redundant roles in plant
943 innate immunity. PLoS Pathog **5**: e1000526

944 **Nohales MA, Kay SA** (2016) Molecular mechanisms at the core of the plant circadian oscillator.
945 Nat Struct Mol Biol **23**: 1061–1069

946 **Nolte C, Staiger D** (2015) RNA around the clock - regulation at the RNA level in biological
947 timing. Front Plant Sci **6**: 311

948 **Perez-Santángelo S, Mancini E, Francey LJ, Schlaen RG, Chernomoretz A, Hogenesch JB,**
949 **Yanovsky MJ** (2014) Role for LSM genes in the regulation of circadian rhythms. Proc
950 Natl Acad Sci U S A **111**: 15166–15171

951 **Plautz JD, Straume M, Stanewsky R, Jamison CF, Brandes C, Dowse HB, Hall JC, Kay SA**
952 (1997) Quantitative analysis of Drosophila period gene transcription in living animals. J
953 Biol Rhythms **12**: 204–217

954 **Romanowski A, Schlaen RG, Perez-Santangelo S, Mancini E, Yanovsky MJ** (2020) Global
955 transcriptome analysis reveals circadian control of splicing events in Arabidopsis thaliana.
956 Plant J **103**: 889–902

957 **Sanchez SE, Petrillo E, Beckwith EJ, Zhang X, Rugnone ML, Hernando CE, Cuevas JC,**
958 **Godoy Herz MA, Depetris-Chauvin A, Simpson CG, et al** (2010) A methyl transferase
959 links the circadian clock to the regulation of alternative splicing. Nature **468**: 112–116

960 **Schlaen RG, Mancini E, Sanchez SE, Perez-Santángelo S, Rugnone ML, Simpson CG,**
961 **Brown JWS, Zhang X, Chernomoretz A, Yanovsky MJ** (2015) The spliceosome
962 assembly factor GEMIN2 attenuates the effects of temperature on alternative splicing and
963 circadian rhythms. Proc Natl Acad Sci U S A **112**: 9382–9387

964 **Semlow DR, Blanco MR, Walter NG, Staley JP** (2016) Spliceosomal DEAH-Box ATPases
965 Remodel Pre-mRNA to Activate Alternative Splice Sites. Cell **164**: 985–998

966 **Seo PJ, Park M-J, Lim M-H, Kim S-G, Lee M, Baldwin IT, Park C-M** (2012) A self-
967 regulatory circuit of CIRCADIAN CLOCK-ASSOCIATED1 underlies the circadian
968 clock regulation of temperature responses in Arabidopsis. Plant Cell **24**: 2427–2442

969 **Shakhmantsir I, Sehgal A** (2019) Splicing the Clock to Maintain and Entrain Circadian
970 Rhythms. J Biol Rhythms **34**: 584–595

971 **Shi Y** (2017) Mechanistic insights into precursor messenger RNA splicing by the spliceosome.
972 Nat Rev Mol Cell Biol **18**: 655–670

973 **Uehara TN, Nonoyama T, Taki K, Kuwata K, Sato A, Fujimoto KJ, Hirota T, Matsuo H,**
974 **Maeda AE, Ono A, et al** (2022) Phosphorylation of RNA Polymerase II by CDKC;2
975 Maintains the Arabidopsis Circadian Clock Period. Plant Cell Physiol **63**: 450–462

976 **Wang B-B, Brendel V** (2006) Genomewide comparative analysis of alternative splicing in
977 plants. Proc Natl Acad Sci U S A **103**: 7175–7180

978 **Wang X, Wu F, Xie Q, Wang H, Wang Y, Yue Y, Gahura O, Ma S, Liu L, Cao Y, et al**
979 (2012) SKIP is a component of the spliceosome linking alternative splicing and the
980 circadian clock in Arabidopsis. Plant Cell **24**: 3278–3295

981 **Wei Y, Yee PP, Liu Z, Zhang L, Guo H, Zheng H, Anderson B, Gulley M, Li W** (2020)
982 NEDD4L-mediated Merlin ubiquitination facilitates Hippo pathway activation. EMBO
983 Rep **21**: e50642

984 **Wilkinson ME, Charenton C, Nagai K** (2020) RNA Splicing by the Spliceosome. Annu Rev
985 Biochem **89**: 359–388

986 **Xu Y-J, Lei Y, Li R, Zhang L-L, Zhao Z-X, Zhao J-H, Fan J, Li Y, Yang H, Shang J, et al**
987 (2017) XAP5 CIRCADIAN TIMEKEEPER Positively Regulates RESISTANCE TO
988 POWDERY MILDEW8.1-Mediated Immunity in Arabidopsis. Front Plant Sci **8**: 2044

Yang Y, Li Y, Sancar A, Oztas O (2020) The circadian clock shapes the Arabidopsis transcriptome by regulating alternative splicing and alternative polyadenylation. J Biol Chem **295**: 7608–7619

Zhan X, Lu Y, Zhang X, Yan C, Shi Y (2022) Mechanism of exon ligation by human spliceosome. Mol Cell **82**: 2769-2778.e4

Zhang S, Liu Y, Yu B (2014) PRL1, an RNA-binding protein, positively regulates the accumulation of miRNAs and siRNAs in Arabidopsis. PLoS Genet **10**: e1004841

Zhang S, Xie M, Ren G, Yu B (2013) CDC5, a DNA binding protein, positively regulates posttranscriptional processing and/or transcription of primary microRNA transcripts. Proc Natl Acad Sci U S A **110**: 17588–17593

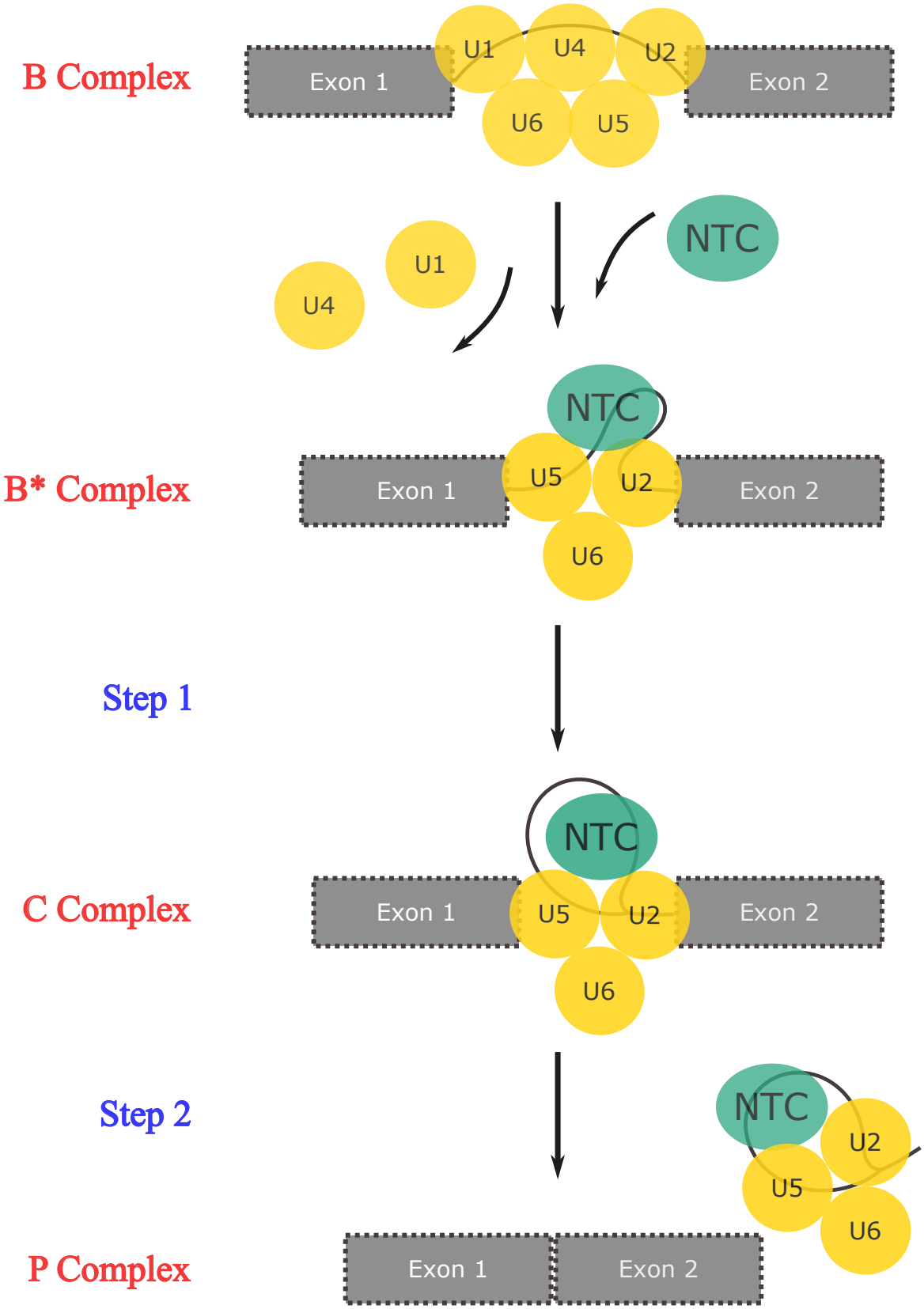
B Complex
Exon 1
U1
U4
U2
Exon 2
U6
U5
NTC
U1
U4
NTC
B* Complex
Exon 1
U5
U2
Exon 2
U6
Step 1
NTC
C Complex
Exon 1
U5
U2
Exon 2
U6
Step 2
NTC
U2
U5
U6
P Complex
Exon 1
Exon 2

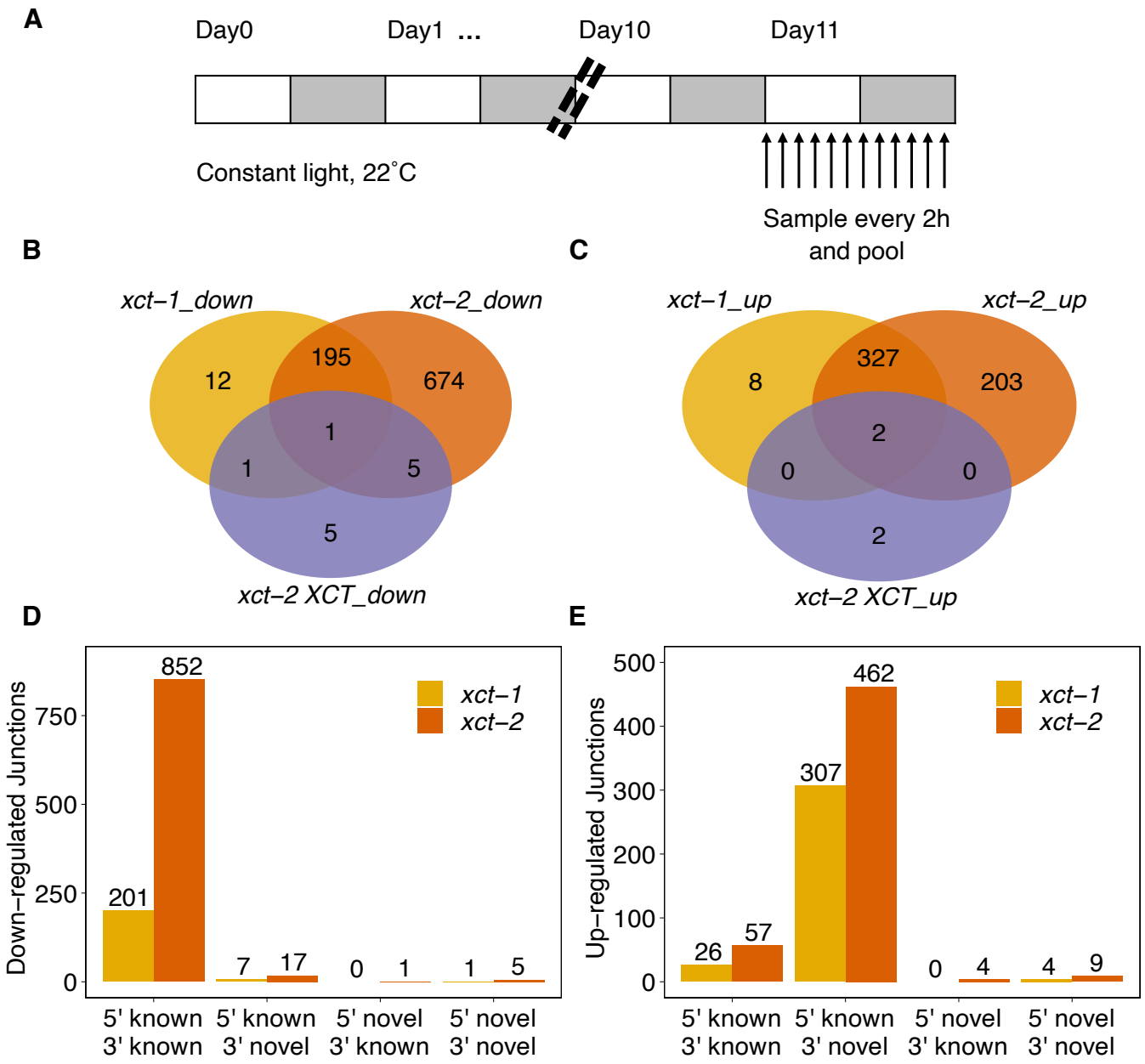
A
Day0
Day1 ...
Day10
Day11
Constant light, 22˚C
Sample every 2h
and pool
B
xct−1_down
xct−2_down
12
195
674
1
1
5
5
xct−2 XCT_down
C
xct−1_up
xct−2_up
8
327
203
2
0
0
2
xct−2 XCT_up
D
Down−regulated Junctions
0
250
500
750
852
201
7
17
0
1
1
5
xct−1
xct−2
5' known 3' known
5' known 3' novel
5' novel 3' known
5' novel 3' novel
E
Up−regulated Junctions
0
100
200
300
400
500
462
307
26
57
0
4
4
9
xct−1
xct−2
5' known 3' known
5' known 3' novel
5' novel 3' known
5' novel 3' novel

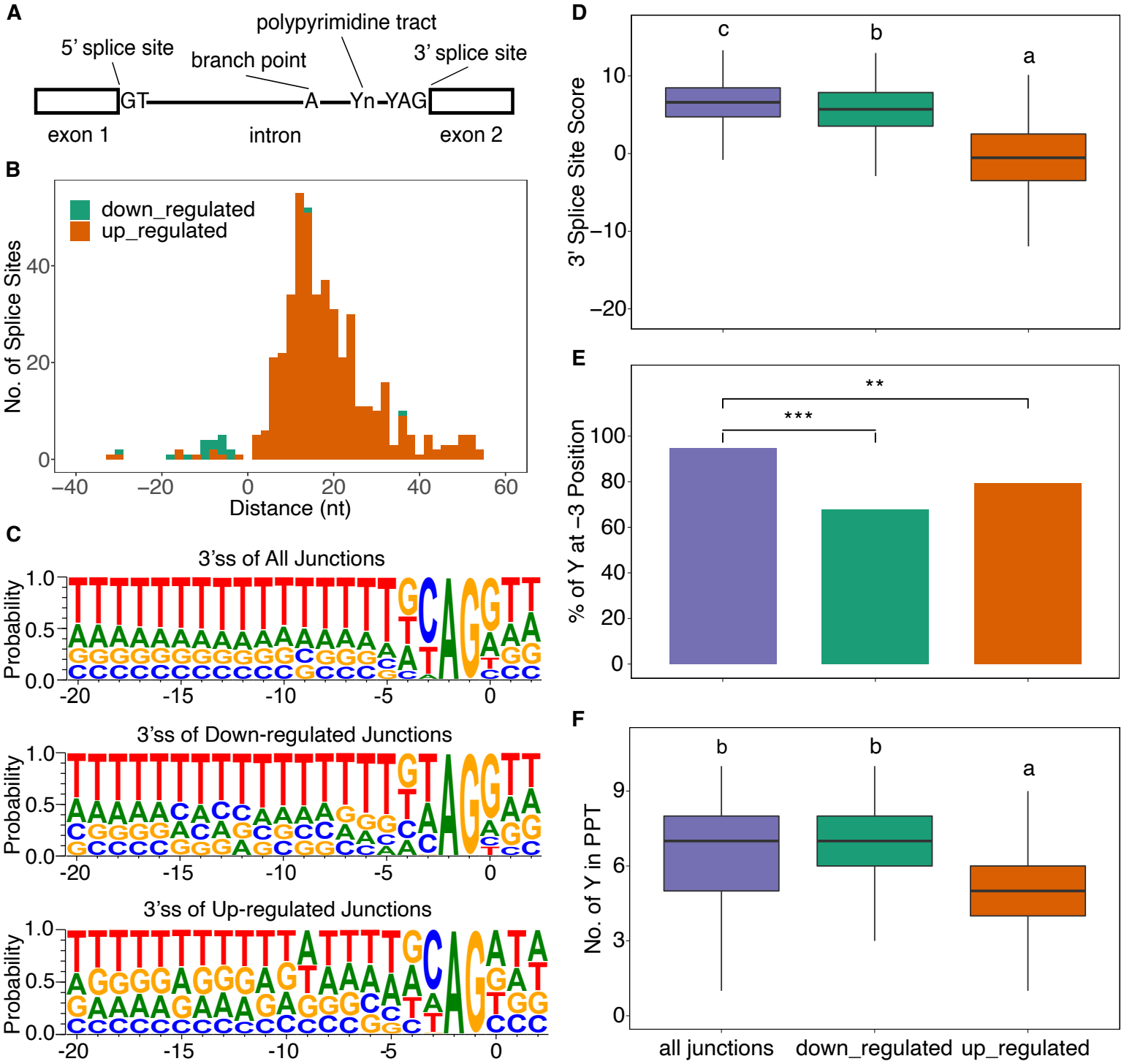
A
5' splice site
branch point
polypyrimidine tract
3' splice site
GT
A
Yn
YAG
exon 1
intron
exon 2
B
down_regulated
up_regulated
No. of Splice Sites
Distance (nt)
C
3'ss of All Junctions
3'ss of Down-regulated Junctions
3'ss of Up-regulated Junctions
Probability
D
3' Splice Site Score
c
b
a
E
% of Y at −3 Position
***
**
F
No. of Y in PPT
b
b
a
all junctions
down_regulated
up_regulated

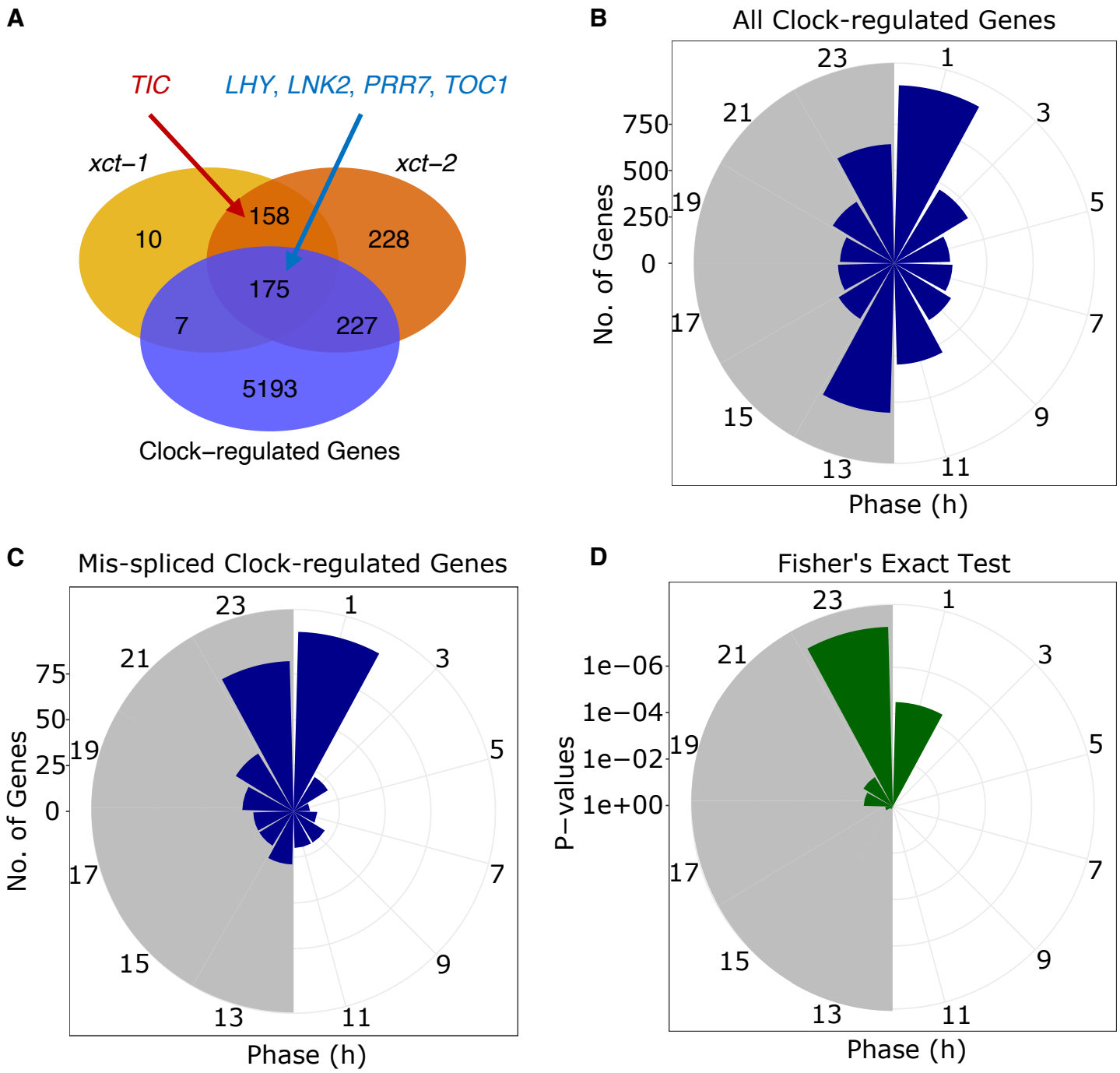
A
TIC
LHY, LNK2, PRR7, TOC1
xct−1
xct−2
10
158
228
175
7
227
5193
Clock−regulated Genes
B
All Clock-regulated Genes
No. of Genes
750
500
250
0
Phase (h)
C
Mis-spliced Clock-regulated Genes
No. of Genes
75
50
25
0
Phase (h)
D
Fisher's Exact Test
P−values
1e−06
1e−04
1e−02
1e+00
Phase (h)

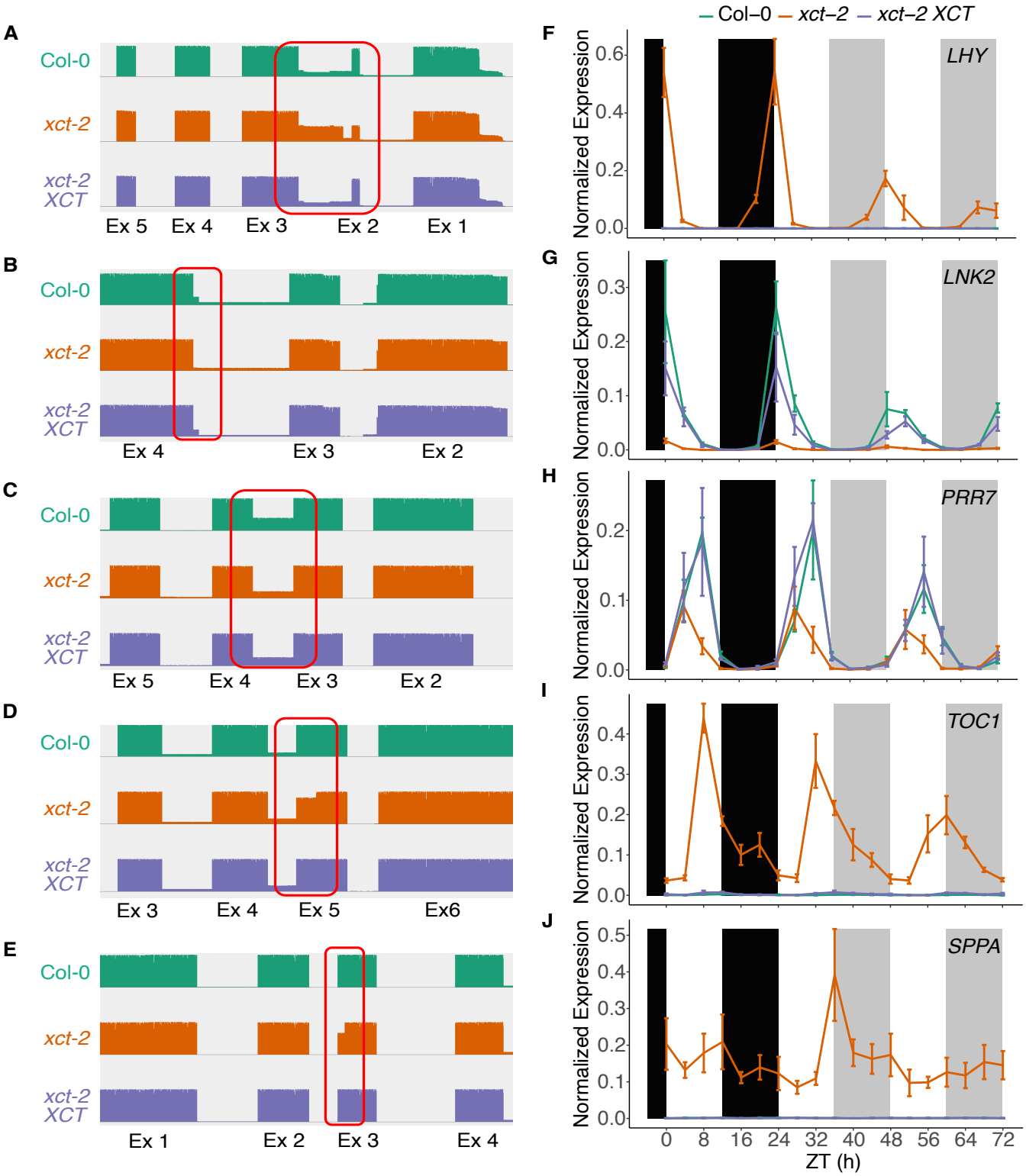
A
Col-0
xct-2
xct-2 XCT
Ex 5
Ex 4
Ex 3
Ex 2
Ex 1
B
Col-0
xct-2
xct-2 XCT
Ex 4
Ex 3
Ex 2
C
Col-0
xct-2
xct-2 XCT
Ex 5
Ex 4
Ex 3
Ex 2
D
Col-0
xct-2
xct-2 XCT
Ex 3
Ex 4
Ex 5
Ex6
E
Col-0
xct-2
xct-2 XCT
Ex 1
Ex 2
Ex 3
Ex 4
Col–0
xct–2
xct–2 XCT
F
LHY
G
LNK2
H
PRR7
I
TOC1
J
SPPA
Normalized Expression
ZT (h)
0
8
16
24
32
40
48
56
64
72

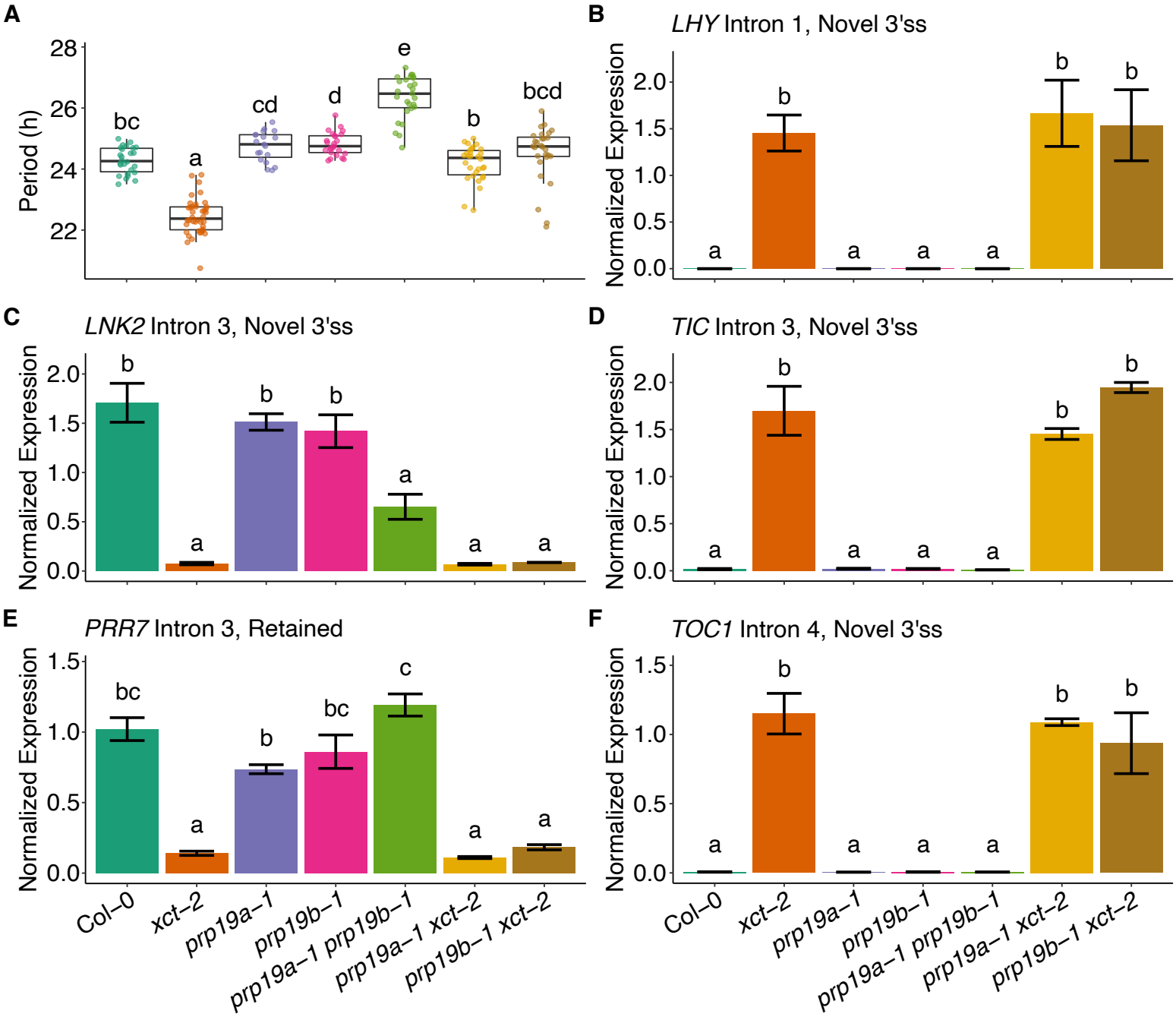
A
Period (h)
28
26
24
22
bc
a
cd
d
e
b
bcd
B
LHY Intron 1, Novel 3'ss
Normalized Expression
2.0
1.5
1.0
0.5
0.0
a
b
a
a
a
b
b
C
LNK2 Intron 3, Novel 3'ss
Normalized Expression
b
a
b
b
a
a
a
D
TIC Intron 3, Novel 3'ss
Normalized Expression
a
b
a
a
a
b
b
E
PRR7 Intron 3, Retained
Normalized Expression
1.5
1.0
0.5
0.0
bc
a
b
bc
c
a
a
F
TOC1 Intron 4, Novel 3'ss
Normalized Expression
a
b
a
a
a
b
b
Col–0
xct–2
prp19a–1
prp19b–1
prp19a–1 prp19b–1
prp19a–1 xct–2
prp19b–1 xct–2

Table 1. XCT physically associates with splicing-related proteins, especially the NTC components, in Arabidopsis. Mass Spectrometry (MS) data showing that spliceosome-associated proteins are significantly more enriched in XCT-YFP-HA-IP than control IP (fold enrichment > 3; *P* -value < 0.05, Welch two sample t.test). The full list of proteins co-purified with XCT are described in Supplemental Dataset 1. Only proteins detected in each biological replicate and with 20 or more total peptides counts are shown.

AGI	*A. thaliana* gene name	*P*- value	fold enrichment	category	*S. cerevisiae* homolog	*H. sapiens* homolog
AT2G21150	XCT	6.21E-04	Inf			FAM50A
AT1G04510	PRP19A/MAC3A/PUB59	1.52E-02	4.2	NTC	Prp19p	PRPF19; PSO4; SNEV
AT2G33340	PRP19B/MAC3B/PUB60	2.17E-03	4.8	NTC		
AT4G15900	PRL1/MAC2	1.24E-02	7.7	NTC	Prp46p	PLRG1
AT1G77180	SKIP/MAC6	1.36E-03	4.9	NTC	Prp45p	SNW1
AT1G09770	CDC5/MAC1	4.06E-03	6.7	NTC	Cef1p	CDC5L
AT1G07360	MAC5A	2.15E-03	8.8	NTC	Ecm2p	RBM22
AT5G41770	CRNK1/MAC10	5.78E-03	7.7	NTC	Clf1p/Syf3	CRNKL1/SYF3
AT3G18790	ISY1/MAC8	1.26E-03	6.1	NTC	Isy1p	ISY1
AT2G38770	EMB2765/MAC7	1.36E-02	4.4	NTC	Cwf11p	AQR
AT5G28740		8.86E-03	4.6	NTC	Syf1p	XAB2
AT3G18165	MOS4	4.09E-03	4.5	NTC	Snt309p	BCAS2/SPF27
AT5G51280		1.65E-02	4.3	other splicing	Dbp2p	DDX41
AT2G47640		4.93E-03	4.3	other splicing	Smd2p	SNRPD2
AT3G26560		8.15E-03	24	other splicing	Prp22p	DHX8
AT1G09760	U2A'	3.51E-02	3.3	U2 complex	Lea1p	SNRPA1